

Turbulence and Ion Acceleration in the Outer Heliosphere

REINALD KALLENBACH¹

International Space Science Institute, Bern, Switzerland

ANDRZEJ CZECHOWSKI

Space Research Centre, Polish Academy of Sciences, Warsaw, Poland

MARTIN HILCHENBACH

Max-Planck-Institut für Sonnensystemforschung, Katlenburg-Lindau, Germany

PETER WURZ

Physikalisches Institut, University of Bern, Switzerland

Abstract. The transport parameters of suprathermal and energetic particles in the heliosphere are intimately linked to the properties of the plasma turbulence in the supersonic solar wind flow and in the subsonic heliosheath plasma flow beyond the termination shock. Based on observations with the magnetometers on board the Helios, ACE, Ulysses, and Voyager spacecraft, and on theoretical calculations, the quantitative evolution of transport parameters of suprathermal particles over heliocentric distances is estimated. From these transport parameters, the stochastic acceleration efficiencies and spatial pressure profiles of suprathermal ions in the solar wind termination region are derived. The scattering mean free path in the heliosheath plasma also yields the injection threshold speed and characteristic time-scales for first-order Fermi acceleration of ions at the termination shock. The theoretical results are compared to observations of suprathermal ions, i.e. the termination shock energetic particles (TSPs) and the Anomalous Cosmic Rays (ACRs), with the Voyager spacecraft in the outer heliosphere, and with data on energetic neutral atoms (ENAs) detected with the CELIAS/HSTOF sensor onboard SOHO and with the ASPERA-3 sensor onboard Mars Express.

7.1 Introduction

The transport of suprathermal charged particles in the magnetized solar wind plasma is qualitatively described by convection, drift, adiabatic deceleration in the expanding solar wind, and by diffusion. The process of diffusion is subdivided into

¹in *The Physics of the Heliospheric Boundaries*, V. Izmodenov and R. Kallenbach (eds.), ISSI Scientific Report No. 5, pp. 203 - 243, ESA-ESTEC, Paris 2006

spatial diffusion and diffusion in momentum space. The basis for a quantitative description of the transport is given by the Parker equation, which may be written in the form

$$\frac{\partial f}{\partial t} + (\mathbf{V} + \mathbf{V}_D) \cdot \nabla f = \nabla \cdot (\mathcal{K} \nabla f) + \frac{v}{3} \frac{\partial f}{\partial v} \nabla \cdot \mathbf{V} + \frac{1}{v^2} \frac{\partial}{\partial v} \left(v^2 D_{vv} \frac{\partial f}{\partial v} \right) + Q - S \quad (7.1)$$

or in other variations. The velocity \mathbf{V} is the convection velocity of the bulk plasma in some reference frame such as the spacecraft frame, the tensor \mathcal{K} describes the spatial diffusion, the parameter D_{vv} the diffusion of a nearly isotropic charged particle distribution in velocity space, and Q and S are source and sink terms such as the creation of ions in the plasma by ionization of neutrals or the reverse process, respectively. The term $(\nabla \cdot \mathbf{V}) v \partial_v f / 3$ describes the adiabatic deceleration (acceleration) in an expanding (converging) plasma flow. The velocity \mathbf{V}_D describes the drift of the suprathermal particles such as magnetic-field gradient or curvature drift. Parker's equation has been developed for theories on cosmic ray transport. It applies for a minority population of particles which are not "members" of the thermal distribution of the bulk plasma. The equation also applies to some extent to particles which are only slightly suprathermal, although the approach breaks down at some lowest energy. Equation (7.1) is usually written in the solar wind rest frame in order to have a nearly isotropic particle distribution in the bulk plasma frame even for the lowest-energy suprathermal particles such as pick-up ions.

The transport parameters \mathcal{K} and D_{vv} of suprathermal ions are usually described in the frame of the quasi-linear theory (QLT), a theory based on the original work by Jokipii (1966). A recent study by Bamert et al. (2004) suggests that the parallel mean free path described by the QLT, $\lambda_{\parallel} = 3v^2 / \left[8\pi\Omega_p^2 \tilde{P}(k) \right]$, describes fairly well the propagation of energetic protons with speed v and angular gyro-frequency Ω_p in the solar wind plasma, if only the Alfvénic fluctuations in slab geometry enter the power spectral density $\tilde{P}(k) = \delta \tilde{B}^2 / B_0^2$ at the resonant wave number $k \approx \Omega_p / v$.

If this result holds for the solar wind termination region, the evolution of the Alfvénic fluctuations with heliocentric distance gives an estimate of the injection threshold for suprathermal ions into first-order Fermi acceleration at the termination shock and for the confinement and build-up of pressure of suprathermal (energetic) particles in the turbulent heliosheath plasma flow. Some uncertainty enters the estimate because it is not entirely clear what happens to the Alfvénic turbulence at the quasi-perpendicular termination shock itself. However, Voyager 1 (Acuña et al., 2006) magnetic field data give some constraints on the order of magnitude of Alfvénic fluctuations in the heliosheath.

This tutorial will be organized as follows: In Section 7.2 we will review the properties of solar wind turbulence and its evolution over heliocentric distance. In Section 7.3, we calculate the injection threshold for first-order Fermi acceleration at the solar wind termination shock as a function of the shock normal angle and as a function of heliolongitude and heliolatitude. In Section 7.4 we will derive the transport parameters \mathcal{K} and D_{vv} and discuss the evolution of suprathermal tails in the ion distributions over heliocentric distance. Section 7.5 discusses the dynamical role of energetic particles near the termination shock. In Section 7.6 numerical simulations of the termination shock reformation and of the microscopic structure are summarized. Section 7.7 contains the conclusions. Appendix 7.A presents a

compact mathematical derivation of the relation of the transport parameters \mathcal{K} and D_{vv} to the power spectral densities of compressive and non-compressive MHD solar wind turbulence, while Appendix 7.B summarizes in detail the mathematical model of magnetohydrodynamic (MHD) turbulence in the supersonic solar wind plasma, which is briefly wrapped up in the following Section.

7.2 Evolution of solar wind turbulence

Present models consider the Alfvén radius – the distance from the Sun, where the bulk solar wind reaches the Alfvén speed – as the “birth place” of Alfvénic solar wind turbulence. This view has been initiated by models that dealt with purely non-compressive fluctuations that propagate in a proton-dominated solar wind with the Alfvén speed $v_A = B_0/\sqrt{\mu_0 n_p m_p}$, where B_0 is the ambient interplanetary magnetic field strength, n_p is the proton density and m_p the proton mass. Once the solar wind has reached the Alfvén speed, the Alfvénic fluctuations cannot return any more to the solar source, and, therefore, the properties of the Alfvénic turbulence in a homogeneous solar wind are determined by the boundary conditions at the Alfvén radius. This situation may approximately be realized in the polar coronal hole regions (vertical axis in Figure 7.1). There, quasi-stationary fast solar wind streams with non-compressional (Alfvénic) fluctuations dominate.

However, there are many more sources of solar wind turbulence outside the Alfvén radius, in particular close to the ecliptic plane (horizontal axis in Figure 7.1). Coronal mass ejections and stream interactions between slow and fast solar wind streams drive compressional fluctuations through interplanetary shocks and global structures such as Co-rotating Interaction Regions (CIRs) and (Global) Merged Interaction Regions (GMIRs).

Furthermore, any anisotropy in particle distributions at speed v , $f(v, \mu) - f(v, -\mu)$, leads to growth of Alfvén waves by the resonance condition $\Omega + k_{\parallel} v \mu - \omega$, where μ is the pitch-angle cosine and k_{\parallel} can have both signs describing Alfvén waves travelling parallel and antiparallel along the ambient magnetic field B_0 . Any spatial pressure gradient of a particle distribution leads to an anisotropy. The contribution of Solar Energetic Particles (SEPs) to the Alfvén wave driving in the inner heliosphere is not yet evaluated sufficiently in the literature.

An example of SEP-driven interplanetary Alfvén waves is shown in Figure 7.2. In panel (B) the increase of Alfvénic wave power above the ambient level of solar wind turbulence due to energetic protons is shown (Bamert et al., 2004). The amplified waves have indeed been identified as being Alfvénic. Panel (C) shows the increase in the power of magnetic fluctuations at an interplanetary quasi-parallel shock, which matches fairly well the model by Vainio and Schlickeiser (1999). The interplanetary shocks driven by coronal mass ejections (CMEs) are presumably strongest close to the Sun at about 4 – 6 solar radii so that most of SEP-driven turbulence may be generated there. This location of maximum shock strength, however, is still outside the Alfvén radius.

The Alfvénic turbulence in the solar wind is anisotropic (Figure 7.3). There are more anti-sunward than sunward propagating waves. This may be a natural consequence of the fact that outward propagating waves have a higher escape prob-

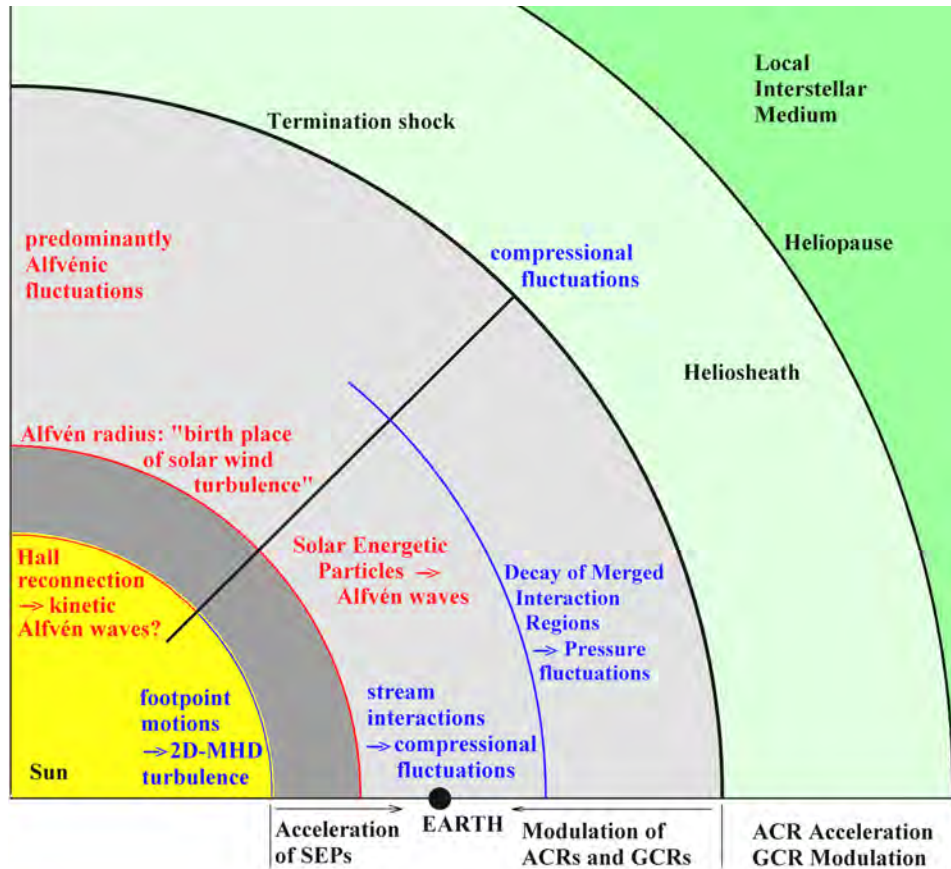


Figure 7.1: Schematic overview of the heliosphere showing some of the most important processes of solar wind turbulence generation.

ability from the region inside the Alfvén radius. On the other hand, SEP-driven Alfvén waves also preferentially propagate anti-sunward.

The generation and amplification of turbulence at a quasi-perpendicular shock such as the solar wind termination shock and near stream interfaces of co-rotating interaction regions (CIRs) has not yet been studied theoretically in detail. However, the data shown in Figure 7.3 suggest that stream interactions decrease the anisotropy, which may be an indicator for the generation of isotropic compressional fluctuations. As outlined by Ness (2006, this volume), the inner heliosheath i.e. the turbulence region downstream of the solar wind termination shock, is indeed a region of strongly compressional turbulence.

In contrast, the polar coronal hole (fast) solar wind is a region with nearly incompressional fluctuations. Horbury and Balogh (2001) have studied the radial evolution of the solar wind turbulence in Ulysses magnetometer data (Figure 7.4). It appears that the turbulence in the inertial range scales with r^{-3} , where r is the heliocentric distance. This scaling corresponds to the so-called WKB-scaling,

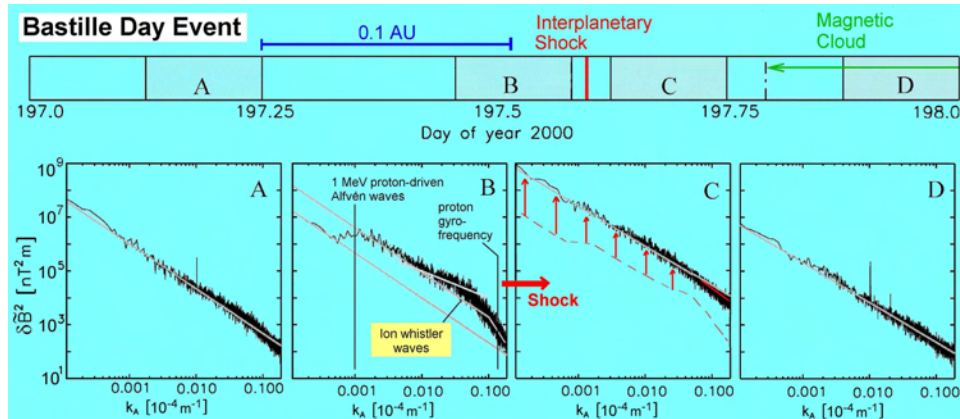


Figure 7.2: Overview of power spectral densities of magnetic field fluctuations near the strongest interplanetary shock during the Bastille Day event (Kallenbach and Bamert, ACE news #91).

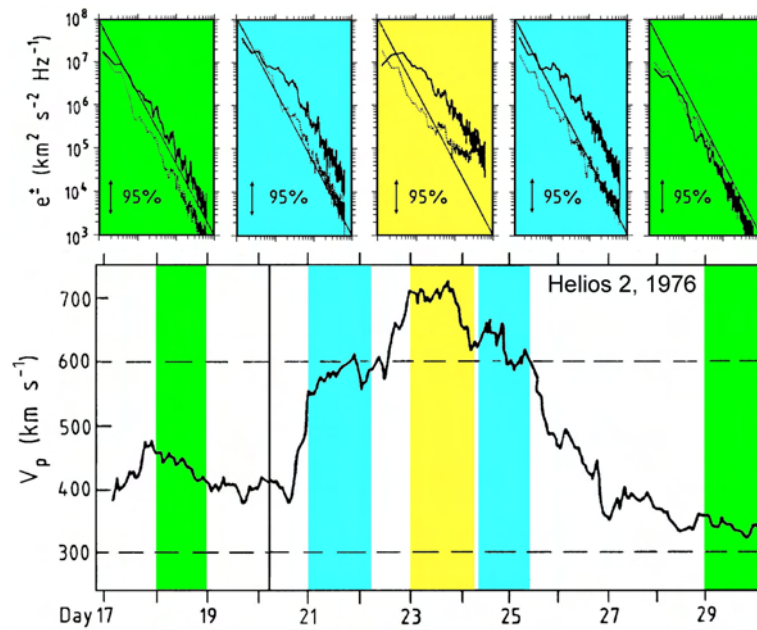


Figure 7.3: Turbulence properties of the solar wind at 1 AU (Tu et al., 1990).

which applies if there are no sources of turbulence, in particular no sources for compressional fluctuations.

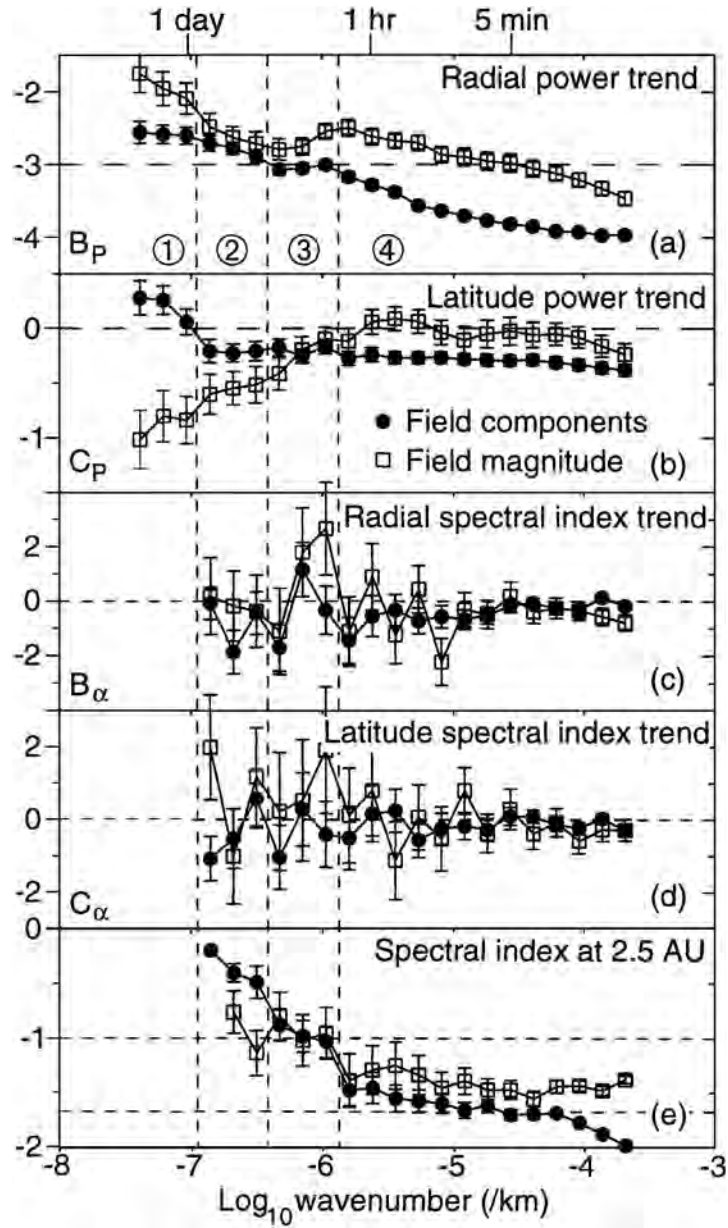


Figure 7.4: Evolution of solar wind turbulence properties between 1.4 and 4.1 AU in polar coronal hole streamers (Horbury and Balogh, 2001). The power of solar wind turbulence follows the law $\log_{10} P = A_P + B_P \log_{10} r + C_P \sin \theta$, where r is the heliocentric distance and θ the heliolongitude. The power spectral index α of the turbulence follows the law $\alpha = A_\alpha + B_\alpha \log_{10} r + C_\alpha \sin \theta$.

A detailed mathematical model of solar wind MHD turbulence is summarized in the Appendix (Section 7.B). The resulting equations of evolution with heliocentric distance are (Equation 7.70):

$$\begin{aligned} \left(\frac{\partial}{\partial t} + \nabla \cdot \frac{\mathbf{U}}{2} + \mathbf{U} \cdot \nabla - \Gamma \frac{U}{r} \right) E_b &= -\frac{E_b^{3/2}}{l_c} + S ; \\ \left(\mathbf{U} \cdot \nabla + \Gamma \frac{U}{r} \right) l_c &= \frac{E_b^{1/2}}{2} - \frac{l_c S}{2E_b} . \end{aligned} \quad (7.2)$$

Here, \mathbf{U} is the solar wind bulk velocity, and the magnetic energy is defined as $E_b = b^2 / (2\mu_0\rho)$, where \mathbf{b} is the amplitude of the magnetic field fluctuations. For slab and 2D-MHD turbulence, the mixing parameter Γ describes the coupling of magnetic and velocity fluctuations. As is derived in the Appendix (Section 7.B), we have $\Gamma = -\sigma_D \cos^2 \Psi$, where $\sigma_D = (r_A - 1) / (r_A + 1)$ with the Alfvén ratio $r_A = E_v / E_b$. The Alfvén ratio gives the ratio between the power per unit mass in the kinetic fluctuations $E_v = v^2/2$ and the magnetic fluctuations E_b . In general, i.e. for $\sigma_D \neq 0$, the coupling between magnetic and kinetic fluctuations depends on the angle Ψ between the plasma flow and the ambient magnetic field.

In the solar wind, we have $\Gamma > 0$ ($\sigma_D < 0$) or $r_A = E_v / E_b < 1$, respectively. For purely Alfvénic fluctuations, we have $\sigma_D = 0$ and, thus, $\Gamma = 0$. This means that Alfvénic fluctuations with $E_v - E_b = 0$ convect unchanged at any angle Ψ in the solar wind plasma as long as the expansion can be neglected. Even at $\Psi = 90^\circ$ magnetic and kinetic fluctuations do not couple.

Without dissipation, sources, or mixing, i.e. $l_c = \infty$, $S = 0$, and $\Gamma = 0$, Equation (7.2) fulfils the familiar WKB solution

$$U \frac{\partial E_b}{\partial r} + \frac{U}{r} E_b = 0 \quad \Rightarrow \quad \frac{E_b}{E_{b0}} = \frac{r_0}{r} \quad \Rightarrow \quad \frac{b^2}{b_0^2} = \left(\frac{r_0}{r} \right)^3 \quad \text{if} \quad \frac{\rho}{\rho_0} = \left(\frac{r_0}{r} \right)^2. \quad (7.3)$$

For $\Psi \approx 0$ and $\sigma_D \approx -1$, i.e. for a solar wind flow parallel to the ambient magnetic field dominated by magnetic fluctuations, we have $\Gamma \approx 1$. In that case it follows that $b/b_0 \propto r_0/r$ as was suggested by Jokipii and Kota (1989) for the polar magnetic field. Such a field with strong magnetic fluctuations enhances cosmic ray transport across the ambient magnetic field. Further out at the Ulysses orbit, where the interplanetary (heliospheric) magnetic field is rather perpendicular, the fluctuations in the coronal hole regions rather follow the WKB solution (Figure 7.4).

For a general $\Gamma \neq 1$, i.e. for a stronger coupling between kinetic and magnetic fluctuations and/or non-Alfvénic fluctuations, and including sources of the form $S = C_S U E_b / r$, the solution of Equation (7.2) is

$$\begin{aligned} \frac{E_b}{E_{b0}} &= \frac{(r_0/r)^{1-\Gamma-C_S}}{1 + A^{-1}C^{-1} \left[(r/r_0)^A - 1 \right]} \propto r^{-(3+\Gamma)/2} \quad \text{for} \quad r \rightarrow \infty; \\ \frac{l_c}{l_{c;0}} &= \left\{ 1 + A^{-1}C^{-1} \left[(r/r_0)^A - 1 \right] \right\}^{1/2} \left(\frac{r_0}{r} \right)^{\Gamma+C_S/2} \rightarrow r^{(1-\Gamma)/4}; \\ A &= \frac{1 + 3\Gamma + 2C_S}{2}; \quad C = \frac{l_{c;0}U}{r_0 E_{b;0}^{1/2}}. \end{aligned} \quad (7.4)$$

All acceleration and modulation processes of Solar Energetic Particles (SEPs), Galactic Cosmic Rays (GCRs), and Anomalous Cosmic Rays (ACRs) involve turbulence in the solar wind and in its source regions. Therefore, the above described evolution of solar wind turbulence, which determines the evolution of transport parameters over heliocentric distance, is essential to understand the behaviour of all suprathermal tails and energetic particle populations, such as ACRs, GCRs, and SEPs, in the heliosphere.

In the next section, the evolution of the parallel mean free path over the heliocentric distance is evaluated in order to estimate the injection threshold for suprathermal ions in the solar wind into the first-order Fermi acceleration process at the solar wind termination shock.

7.3 Injection threshold at the termination shock

Transport parameters of energetic ions are usually described in the frame of the quasi-linear theory (QLT), a theory based on the original work by Jokipii (1966). A recent study by Bamert et al. (2004) suggests that the parallel mean free path derived from the QLT,

$$\lambda_{\parallel} = \frac{3}{16} r_g^2 P^{-1} (r_g^{-1}) = \frac{3(s-1)}{16} r_g \left(\frac{2\pi r_g}{l_{c;A}} \right)^{1-s} \zeta_A^{-1}, \quad \zeta_A = \frac{\langle \delta B_A^2 \rangle}{B_0^2} \propto E_b, \quad (7.5)$$

describes fairly well the propagation of energetic protons with speed v and angular gyro-frequency Ω_p in the solar wind plasma, if only the Alfvénic fluctuations in slab geometry enter the power spectral density $P(k_r) = \delta \tilde{B}^2(k_r)/B_0^2$ at the resonant wavenumber $k_r \approx \Omega_p/v = r_g^{-1}$. We assume that the power spectral density of the Alfvénic fluctuations follow a power law, e.g. a Kolmogorov law with spectral index $s = 5/3$, and that there are as many forward as backward travelling waves. The parameter ζ_A describes the square of the total Alfvénic fluctuation amplitude in relation to the square of the ambient magnetic field amplitude B_0 and is proportional to the power per unit mass in the magnetic fluctuations E_b used in Equation (7.2). The correlation length or outer scale $l_{c;A}$ of the Alfvénic fluctuations can be interpreted as the maximum wavelength of the turbulence, structures larger than $l_{c;A}$ are ordered, while structures smaller than $l_{c;A}$ are chaotic or turbulent. Near Earth, the Alfvénic correlation length is about $l_{c;A} \approx 0.03\text{AU}$ (Goldstein et al., 1995).

The above expression for λ_{\parallel} is derived in Appendix 7.A.3. In the literature, however, one often finds the pre-factor $3/(8\pi)$ instead of $3/16$.

7.3.1 Evolution of turbulence with heliocentric distance

The parallel mean free path is the basic transport parameter for charged-particle transport in the supersonic solar wind. It is also one reference for charged particle transport in the heliosheath and, therefore, can be used to estimate the injection threshold speed for ions to be diffusively accelerated at the termination shock. Diffusive acceleration at the termination shock occurs when the diffusion speed in the heliosheath overcomes the steady-state convection speed of suprathermal ions.

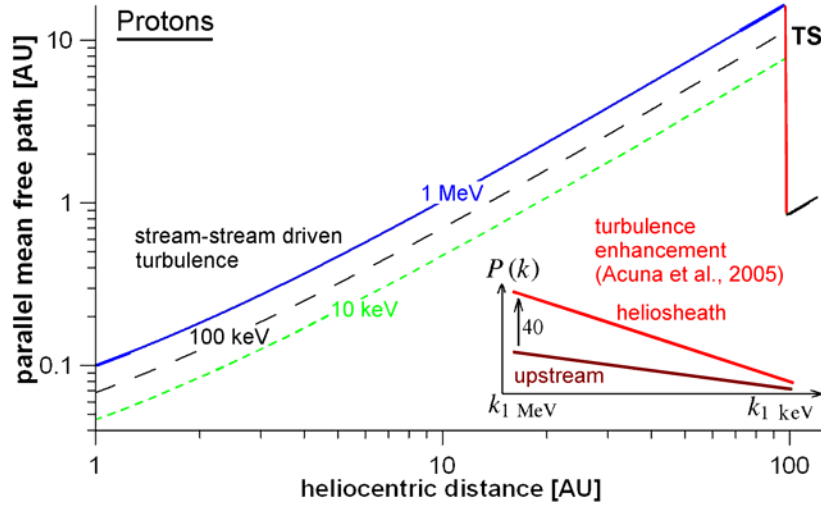


Figure 7.5: Evolution of the parallel mean free path of protons with heliospheric distance in the ecliptic plane. The inset qualitatively represents the increase in turbulent power observed by the Voyager 1 magnetometer (see Acuña et al., 2006, for the precise data).

And this diffusion speed is related to the parallel mean free path. Therefore, the calculation of the evolution of the turbulent power with heliocentric distance is the basis to evaluate the transport parameters in the solar wind termination region.

The parallel mean free paths for different proton energies at 1 AU are taken from the observations by Bamert et al. (2004) of the upstream region of the Bastille Day shock (see Figure 7.5 for the values). The evolution of the Alfvénic component of solar wind turbulence is calculated according to Equation (7.4). This equation is equivalent to the model of Zank et al. (1996a). As in their work, we assume a constant mixing ratio $\Gamma = 0.2$ between magnetic field and velocity fluctuations in the solar wind. The parameter Γ is then defined as $\Gamma = \langle -\sigma_D \cos^2 \Psi \rangle$ (see Eq. 7.65), where σ_D is the Alfvénicity and the brackets mean the average over the heliocentric distance. The assumption of constant Γ allows for an analytical solution of the problem. Note, that the pick-up ion driven magnetohydrodynamic (MHD) turbulence is not important for the mean free paths of the higher-energetic particles because these waves are at higher frequencies. However, these MHD-waves partly heat the solar wind and actually mainly heat the pick-up ions themselves (Isenberg et al., 2003; Chalov et al., 2006).

Some uncertainty enters the estimate of turbulent power in the heliosheath because it is not entirely clear what happens to the Alfvénic turbulence at the quasi-perpendicular termination shock itself. Voyager 1 magnetic field data give some constraints on the order of magnitude of Alfvénic fluctuations in the heliosheath as shown in Figure 7.5. The estimate of the downstream parallel mean free path is not obvious, however, as it is not clear whether the amplification of Alfvénic turbulent power corresponds to the factor 40 observed by Voyager 1 for the total amplification

of magnetic turbulent power. However, the gradients of the energetic particle flux at different energies in the heliosheath suggest approximate agreement with the assumption that the Alfvénic turbulent power also increases by a factor close to 40 at the termination shock. Figure 7.6 shows the Voyager data and the derivation of a mean free path by applying Equation (7.31) to the downstream region. The question of why the flux of energetic particles still increases in the heliosheath has been interpreted in different ways. As depicted in Figure 7.7, McComas and Schwadron (2006) suggest that the most efficient acceleration of Anomalous cosmic rays (ACRs) and Termination Shock Energetic Particles (TSPs) mainly takes place at the “flanks” of the heliosphere because the magnetic field lines connecting to the termination shock are longest and most time is available to accelerate ions to high energies. As the termination shock is typically closest to the Sun at the nose (apex), the connecting lines are longest for the regions at heliolongitudes 90° away from the nose, as should become clear from the geometry in Figure 7.7 (*left*). In the nose region, where Voyager 1 has crossed the termination shock, the flux tubes connecting to the shock become longer and longer while travelling into the heliosheath. This explains the increasing flux of TSPs/ACRs. McComas and Schwadron (2006) also assume that the injection threshold into first-order Fermi acceleration is lower at the “flanks” because the termination shock is less perpendicular. These ideas have in fact already been formulated by Chalov (1993; 2000; 2005), Chalov and Fahr (1996; 2000), and Chalov et al. (1997). We will get to the variation of the injection threshold with heliolongitude in the next Section.

Alternatively, the TSP/ACR flux could increase while penetrating the downstream region of the termination shock because of stochastic acceleration in the compressional fluctuations of the heliosheath plasma. Decker et al. (2005) originally suggested that the suprathermal ions behave like an ideal gas which gets compressed during the transition from the upstream solar wind to the heliosheath, and that first-order Fermi acceleration plays a minor role. We will get to this hypothesis in Section 7.4.

7.3.2 The injection threshold as a function of the shock normal angle

According to Giacalone and Jokipii (1999), the threshold for injection of suprathermal ions into the first-order Fermi acceleration process at a shock with upstream solar wind speed V_1 in the shock frame is

$$v_{\text{inj}} = 3V_1 \left[1 + \frac{(\kappa_A/\kappa_{\parallel})^2 \sin^2 \Psi + (1 - \kappa_{\perp}/\kappa_{\parallel})^2 \sin^2 \Psi \cos^2 \Psi}{[(\kappa_{\perp}/\kappa_{\parallel}) \sin^2 \Psi + \cos^2 \Psi]^2} \right]^{1/2}; \quad (7.6)$$

Here, κ_{\parallel} and κ_{\perp} are the spatial diffusion parameters parallel and perpendicular to the magnetic field, and κ_A is the antisymmetric component of the diffusion tensor. See Appendix 7.A.4 for a derivation of Equation (7.6) and for the expressions for κ_{\perp} and κ_A for the case in which the gyroradius r_g of the ion at speed v is small compared to the parallel mean free path λ_{\parallel} .

Figure 7.8 shows the injection threshold (Equation 7.6) for protons as a function

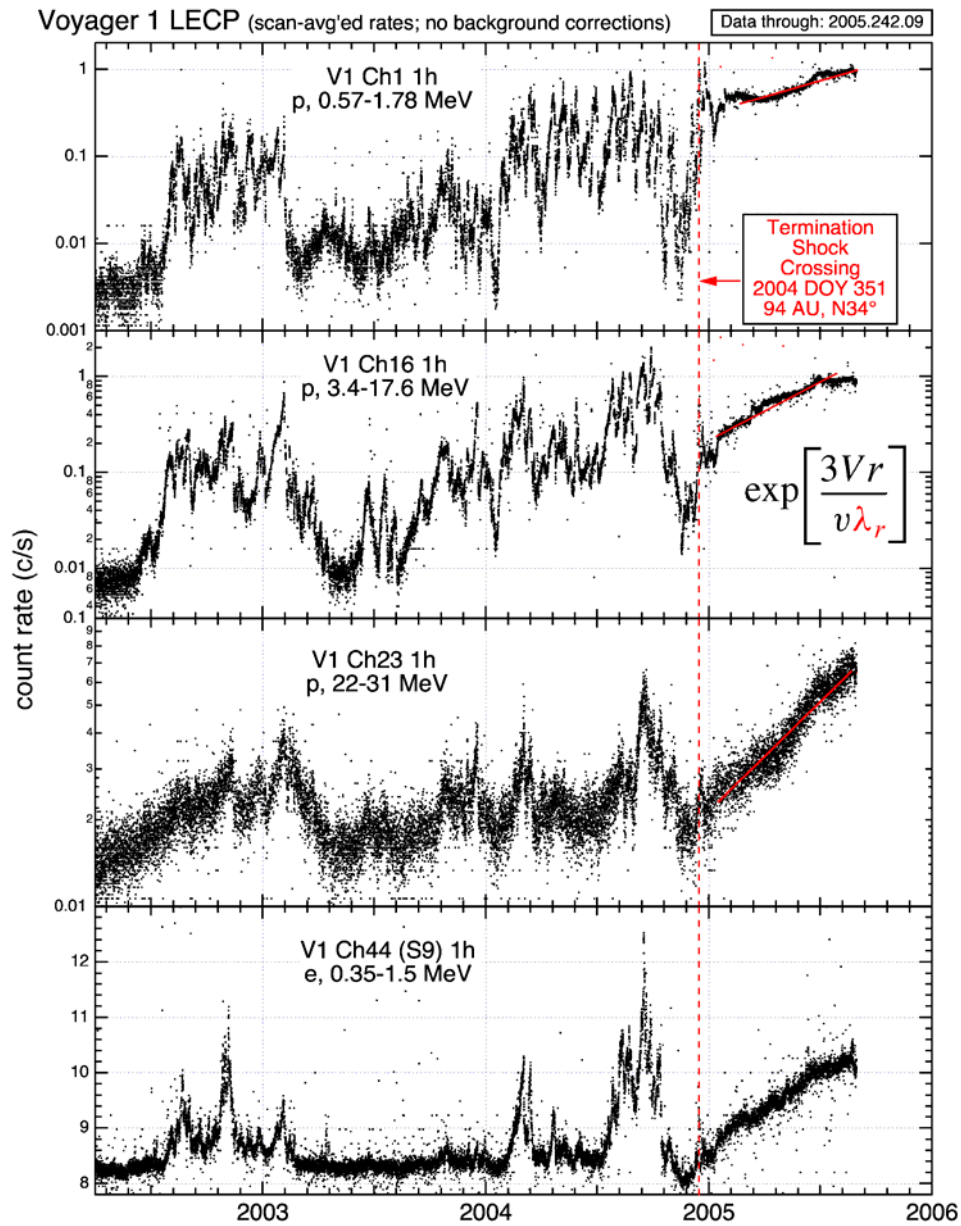


Figure 7.6: Spatial variation of energetic particle flux near the solar wind termination shock. The gradients of the downstream flux can be translated to a parallel mean free path of 0.2 AU for 1 MeV protons, if the magnetic field deviates on average by about 6° from the shock surface as measured by Burlaga et al. (2005) with the magnetometer onboard Voyager 1. For a strict Parker magnetic field angle of $\Psi \approx 89.3^\circ$ and a totally spherical termination shock, the radial mean free path $\lambda_r \approx \lambda_{\parallel} \cos^2 \Psi + \lambda_{\perp} \sin^2 \Psi$ would yield $\lambda_{\parallel} \approx 15$ AU for 1 MeV protons. However, this seems unrealistic, so that $\lambda_{\parallel} \approx 0.2$ AU can be taken as a baseline value. http://sd-www.jhuapl.edu/VOYAGER/images/vgr_qlp/v1_lecp/

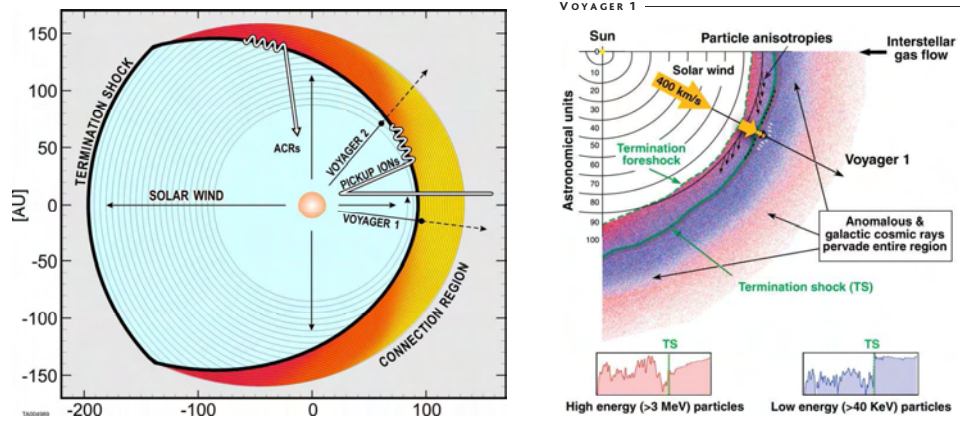


Figure 7.7: *Left*: Schematic geometry of the *termination shock* and the heliospheric magnetic field (McComas and Schwadron, 2006). *Right*: Description of the solar wind termination region by Decker et al. (2005).

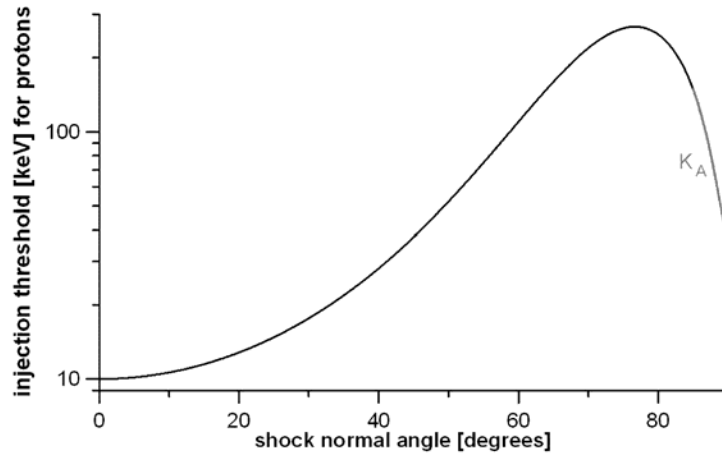


Figure 7.8: Injection threshold into first-order Fermi acceleration of protons at the solar wind termination shock as a function of the shock normal angle.

of the shock normal angle Ψ , based on the turbulence levels that determine the parallel mean free paths in Figure 7.5. The limiting cases are angles between the ambient magnetic field \mathbf{B}_0 and the shock normal angle of $\Psi = 90^\circ$ and $\Psi = 0^\circ$. This yields injection threshold speeds $v_{\text{inj}}(\Psi = 90^\circ) = 3V_1\lambda_{\parallel}/r_g$ and $v_{\text{inj}}(\Psi = 0^\circ) = 3V_1$. The decrease of the injection threshold at $\Psi = 90^\circ$ with respect to $\Psi \approx 80^\circ$ comes from the dominance of the term with κ_A . The return of the ions from the downstream plasma at $\Psi \approx 90^\circ$ is a combination of gyration and perpendicular scattering, which is more efficient than the perpendicular scattering at $\Psi \approx 80^\circ$. It is interesting that the termination shock with $\Psi \approx 90^\circ$ is particularly well suited for injection because the process of pre-acceleration during multiple reflections also works best at $\Psi \approx 90^\circ$ (le Roux et al., 2000), in particular if the scale size of the shock ramp is of the order of the electron inertial length (see Section 7.6).

The expressions in Equation (7.6) correspond to the classical hard-sphere scattering theory, which is only valid if the gyro-radius of the ions, r_g , is larger than the correlation length of the turbulence (Giacalone and Jokipii, 1999). This is not the case in the supersonic upstream solar wind, but may be the case in the downstream thermalized heliosheath plasma (Burlaga et al., 2005). The correlation length may be of the order of the gyro-radius of the bulk protons, which is shorter than the gyro-radius of suprathermal and energetic particles.

7.4 Evolution of suprathermal tails

We solve the Parker equation (7.1) by neglecting spatial diffusion and drift. We assume spherical symmetry and constant solar wind speed. We consider momentum diffusion in compressional turbulence regions which are larger than the mean free path for pitch-angle scattering and neglect momentum diffusion in Alfvénic turbulence (see Section 7.A). For the momentum diffusion parameter we assume that it scales as $D_{vv} \propto r^{-1}v^2$. Any scaling law of D_{vv} close to r^{-1} may be approximated over some range of heliocentric distance by r^{-1} . Observations point towards $D_{vv} \propto r^{-0.7}v^2$ (see Chalov, this volume, and references therein), but the case $D_{vv} \propto r^{-1}v^2$ can be solved analytically because all terms in the Parker equation (7.1) get the same power in r . This leads to an ordinary differential equation in v . We first solve the homogeneous part of the Parker equation (7.A), i.e. with $Q = 0$ and $S = 0$, and then add a source $Q_{\text{PUI}}(\mathbf{r}, v)$ of freshly ionized pick-up ions. The Parker equation is rewritten in speed units $u = v/V_{\text{SW}}$ and radius $\rho = r/1\text{AU}$. In these normalized units the momentum diffusion parameter has the form $D_2\rho^{-1}u^2$, where D_2 is dimensionless.

We obtain a homogeneous solution f_{hom} :

$$-\frac{\partial f}{\partial \rho} + \frac{1}{\rho} \frac{2u}{3} \frac{\partial f}{\partial u} + \frac{D_2}{\rho} \frac{1}{u^2} \frac{\partial}{\partial u} \left[u^4 \frac{\partial f}{\partial u} \right] = 0 \quad \Rightarrow \quad f_{\text{hom}}(u, \rho) = f_0 \rho^{-\beta} u^{-\alpha}$$

with $\beta = \frac{2}{3}\alpha - \alpha(\alpha - 3)D_2$ or $\alpha \approx 3 + \frac{2}{3D_2} - \frac{3\beta}{2 + 9D_2}$, (7.7)

where the approximation for α applies as long as $3\beta/(2 + 9D_2) \ll 3 + 2/(3D_2)$.

The pre-factor f_0 is determined from the local source of freshly ionized interstellar hydrogen atoms. This source scales as ρ^{-2} outside the ionization cavity

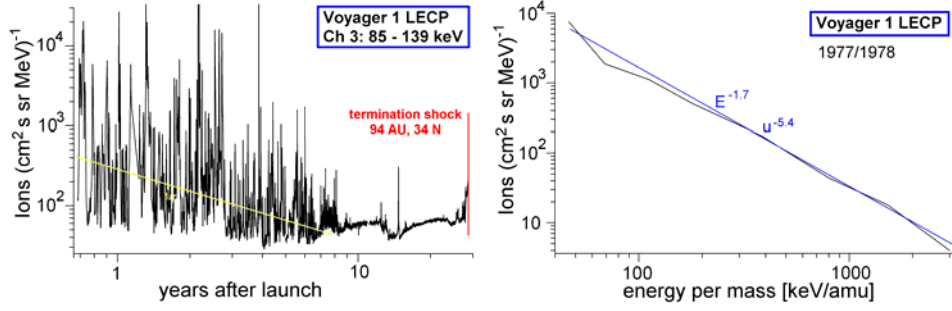


Figure 7.9: Evolution of the flux of suprathermal ions with heliocentric distance ρ from uncalibrated data of the Low Energy Charged Particle (LECP) instrument from the project homepage at Caltech. Voyager 1 moves in average about 3 AU per year. Despite the large variations due to events such co-rotating and merged interaction regions, the mean scaling may be close to ρ^{-1} as denoted by the yellow line. A spectral index $\alpha = 5.4$ of the phase space density seems to be fairly typical.

around the Sun extending out to about 7.5 AU. For interstellar helium atoms, the ρ^{-2} scaling is valid further inwards, in particular in the upwind direction of the interstellar medium, i.e. $Q(u, \rho) = \rho^{-2}q(u)$ for $\rho > 1$. The inhomogeneous solution f_{inhom} then scales as ρ^{-1} i.e. $\beta = 1$.

Trusting the simplified model typical values of D_2 can be derived from the observed spectral index of suprathermal tails. They are in the range $\alpha \approx 5...6$ (Gloeckler, 2003). For a momentum diffusion parameter $D_2 \approx 0.2$ (and $\beta = 1$) the spectral index is $\alpha \approx 5.4$. Note that α cannot be smaller than 5. This is the limit, when stochastic acceleration becomes the dominant term in the transport equation, i.e. $D_2 > 1$. In that case, the quasi-linear description breaks down and one gets a cascade in speed represented by a phase space density scaling as v^{-5} (Fisk et al., 2006). Figure 7.9 shows the data of the Voyager 1 LECP instrument which supports the idea that the suprathermal ion flux scales on average inversely with heliocentric distance, and that a spectral index of 5.4 of the phase space density is fairly typical.

Decker et al. (2005) have suggested that first-order Fermi acceleration at the termination shock plays a minor role for ACRs. Instead, stochastic acceleration in the heliosheath could be an important process. As the momentum diffusion parameter is already $D_2 \approx 0.2$ in the region upstream of the termination shock, it could easily be larger than unity in the heliosheath plasma and make stochastic acceleration very efficient.

It is instructive to evaluate the acceleration time scales for first-order Fermi acceleration at the termination shock with stochastic acceleration (second-order Fermi) in the heliosheath. The time scale for first-order Fermi acceleration is (Kallenbach et al., 2005, and references therein):

$$t_{\text{acc}} = \frac{3}{V_{\text{up}} - V_{\text{ds}}} \int_{v_0}^{v_1} \left(\frac{v\Lambda_{\text{r;up}}}{3V_{\text{up}}} + \frac{v\Lambda_{\text{r;ds}}}{3V_{\text{ds}}} \right) \frac{dv}{v} \Rightarrow$$

$$\tau_{\text{acc;F1}} := \frac{dt_{\text{acc}}}{dv} v \approx \left(\frac{E}{1\text{MeV}} \right)^{2/3} \cos^2 \Psi \left(\frac{A}{Q} \right)^{1/3} \text{ yr} , \quad (7.8)$$

For this rough estimate, mean free paths of order 0.5 AU for protons with 1 MeV energy have been assumed. Compared to this, the acceleration time scale for stochastic acceleration in compressional fluctuations in the upstream slow solar wind with $D_2 \approx 0.2$ is about 4 years ($\rho \approx 100$). This is derived from Equation (7.7), which is written in units of the solar wind convection time scale near Earth. If the compressional fluctuations are stronger by a factor 40 in the heliosheath compared to the upstream solar wind, the acceleration time scale may be about 0.1 year at any energy and mass-per-charge ratio of the ions. This shows that at the high energies in particular stochastic acceleration may well compete with first-order Fermi acceleration.

Note that only in the slow solar wind is the momentum diffusion parameter as large as $D_2 \approx 0.2$, while the fast solar wind has mainly Alfvénic fluctuations, and D_2 is much smaller. If stochastic acceleration is the main process to energize the ACRs, their source is concentrated around the ecliptic plane.

7.5 The dynamical role of energetic particles near the termination shock

Energetic particles near the termination shock can influence the structure of the shock and in a self-consistent manner their own intensity. The mean free path of energetic particles is usually much larger than the scale size of the shock ramp and their energy is much higher than the electric cross-shock potential. Therefore, they move rather freely over the shock layer, i.e. they penetrate from the downstream region far into the upstream region before they are scattered and convected back over the shock into the downstream region. While they are scattered they transfer momentum to the upstream plasma and slow down the upstream plasma if their pressure is comparable to the bulk plasma pressure. A shock precursor is formed and the subshock compression ratio is reduced.

Whenever there is a spatial gradient in energetic particle distributions, there is an anisotropy in the distribution observed in the plasma frame. These anisotropies lead to the generation of plasma waves. These plasma waves cascade and convect over the shock to the downstream region and, consequently, increase the injection threshold for first-order Fermi acceleration and thus limit the energetic particle intensity. These phenomena will be discussed in the next two subsections.

7.5.1 Self-consistent limitation of the TSP flux?

The influence of self-generated upstream waves on the injection threshold for termination shock energetic particles (TSPs) is described in Kallenbach et al. (2005). The termination shock may on average mostly have shock normal angles of $\Psi \approx 80^\circ \pm 5^\circ$. In that range of angles Ψ , if $\cos^2 \Psi > r_g^2 / \lambda_{\parallel}^2$, the term $\cos^2 \Psi$ in

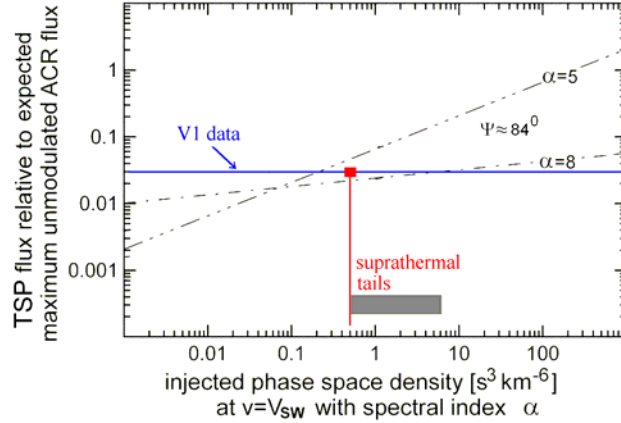


Figure 7.10: The flux of particles accelerated by the first-order Fermi process does not increase proportionally with the flux of injected suprathermal tails because the higher flux of energetic protons generates waves, which in turn increase the injection threshold for first-order Fermi acceleration. The red line denotes the minimum pre-factor $f_0\rho_{\text{TS}}^{-1}$ of the proton phase space density injected at the termination shock, where it is assumed that the proton suprathermal tails observed by Gloeckler (2003) scale in the heliosphere as $f_0\rho^{-1}u^{-\alpha}$. The spectral index of the phase space densities α of the suprathermal tails is typically between 5 and 8. The TSP flux is normalized to the typical unmodulated flux of the ACRs. The proton TSP phase space density at 1 MeV (*blue line*) observed by Stone et al. (2005) is $10^{-5} \text{ s}^3 \text{ km}^{-6}$.

the denominator of the expression for the injection threshold (Eq. 7.6) eventually dominates, so that the injection condition becomes

$$v_{\text{inj}} = 3V_1 r_g / (\lambda_{\parallel} \cos^2 \Psi) . \quad (7.9)$$

This is the injection threshold condition used in Kallenbach et al. (2005). If $\cos^2 \Psi < r_g^2 / \lambda_{\parallel}^2$, this evaluation has to be modified. For an ideal stationary spherical termination shock and a heliospheric magnetic field in the form of a Parker spiral, the self-limitation of energetic particle intensity would occur because upstream energetic protons drive turbulent waves. The amplification of the power spectral density of Alfvénic turbulence is of order $G_A(k) = 1500 \cos \Psi (k/k_{1 \text{ MeV}})^{\gamma_{\text{sh}} - 13/3}$ (Kallenbach et al., 2005), where γ_{sh} is the spectral index of first-order Fermi accelerated particles, $\gamma_{\text{sh}} = 3\xi_{\text{sh}} / (\xi_{\text{sh}} - 1)$ with $\xi_{\text{sh}} = V_{\text{up}} / V_{\text{ds}} = n_{\text{ds}} / n_{\text{up}}$ the shock compression ratio. The wave number $k_{1 \text{ MeV}}$ is approximately the wave number of Alfvén waves which resonate with protons at 1 MeV energy. The amplified Alfvén waves are transmitted through the termination shock and, thus, decrease the parallel mean free path, λ_{\parallel} , in the heliosheath. This increases the injection threshold and consequently decreases the energetic particle flux – a self-limiting process. This self-limitation becomes evident in Figure 7.10. It seems that it may be hard to reach the ACR flux levels by first-order Fermi acceleration at a homogeneous termination shock. Even at high injection phase space density (ordinate in Figure 7.10) the TSP flux does not reach the unmodulated ACR flux (unity on

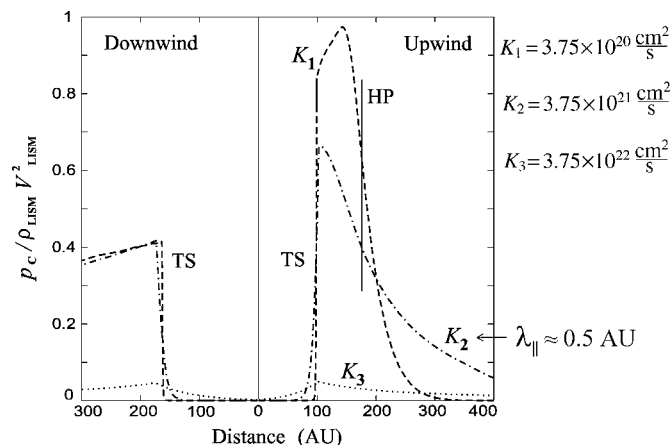


Figure 7.11: Pressure build-up of energetic particles in the heliosheath (Alexashov et al., 2004).

the abscissa of Figure 7.10) originally expected to be observed at the termination shock. The observed level of TSP flux at the termination shock (Stone et al., 2005) in fact matches the model shown in Figure 7.10 (line for 1 MeV particles). Perhaps, additional stochastic acceleration in the heliosheath is necessary to reach the unmodulated ACR level (Kallenbach et al., 2005).

Another possibility is that there are areas of *injection at low turbulence* levels and other areas of *acceleration at high turbulence* levels causing short acceleration time scales. In this way, the unmodulated ACR flux may be reachable by the first-order Fermi process at the termination shock.

7.5.2 ACR pressure build-up in the heliosheath

Figure 7.11 shows the pressure build-up of TSPs and ACRs in the heliosheath according to numerical simulations by Alexashov et al. (2004). The parameter with index 2 corresponds to the evolution of the mean path over the heliocentric distance displayed in Figure 7.5. The parallel mean free path is in that case very roughly about $\lambda_r \approx \lambda_{\parallel} \approx 0.5$ AU for protons at 1 MeV energy in the heliosheath. This in fact matches the observed gradients of the TSP/ACR flux in the heliosheath after Voyager 1 had crossed the solar wind termination shock (Stone et al., 2005). For this parameter set, the TSP/ACR pressure builds up to a significant fraction of the dynamical pressure of the neutral gas component of the Local Interstellar Medium (LISM).

7.5.3 Comparison to data

In order to compare the model results to real data one must know the solar wind parameters and the flux and spectra of suprathermal ions in the outer heliosphere for regions both upstream and downstream of the termination shock, i.e. in the heliosheath.

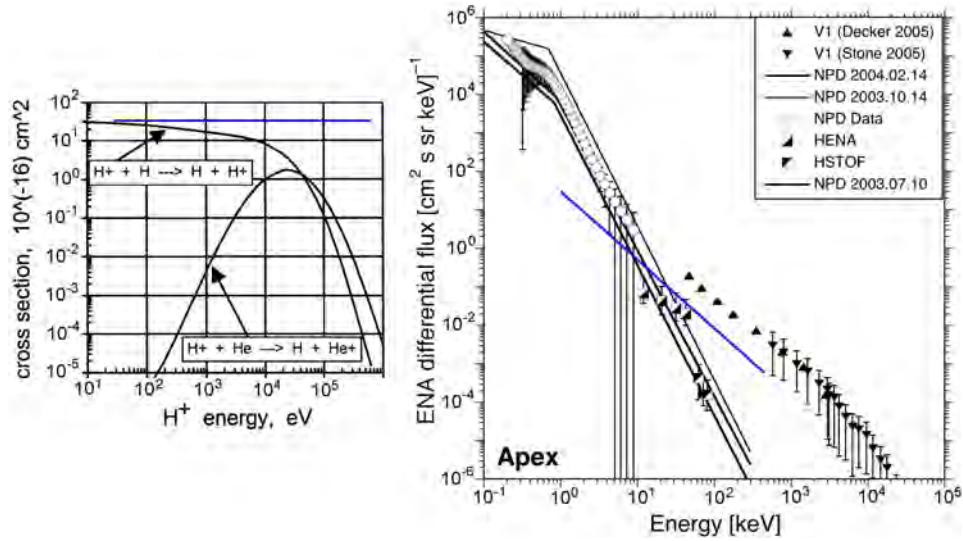


Figure 7.12: Voyager 1 in-situ ion flux data (Stone et al., 2005) from the heliosheath plasma and “remote-sensing” energetic neutral atom data from CELIAS/HSTOF (see also Czechowski et al., this volume), HENA IMAGE data (E. Roelof, private communication), and Mars Aspera-3 data (NPD, Galli et al., 2006). The blue line indicates the model proton spectra in the heliosheath for the injection of the minimum flux of suprathermal tails in the slow solar wind $f = f_0 \rho^{-1} u^{-5}$, $f_0 (u = 1) \approx 50 \text{ s}^3$ (Gloeckler, 2003), and an enhancement of their flux by about a factor 10 at the termination shock. That HSTOF data are below the blue line is due to the fact that the charge exchange cross section decreases at higher energies, as is illustrated in the left panel (Gruntman et al., 2001).

Until December 2004, only energetic neutral atom (ENA) observations for H and He by CELIAS/HSTOF were available to analyze suprathermal ion flux data in the heliosheath. The flux of ENAs near Earth’s orbit created from the suprathermal ion tails anywhere in the heliosphere is modelled in detail by Gruntman et al. (2001), Czechowski et al. (this volume), and Kallenbach et al. (2005). Since the crossing of the termination shock by Voyager 1 (Stone et al., 2005) in December 2004, there are in-situ measurements of suprathermal ion distributions in the heliosheath plasma. Figure 7.12 demonstrates that estimates of the suprathermal ion flux in the heliosheath from CELIAS/HSTOF data are in agreement with the in-situ measurements. Some new data have been contributed by the Neutral Particle Detector (NPD) onboard Mars Express. At low energies ($< 10 \text{ keV}$), the phase space densities of hydrogen atoms are definitely higher than the values derived from pre-acceleration in the supersonic solar wind and acceleration at the termination shock. This indicates that further stochastic acceleration of low-energy protons takes place in the heliosheath. In fact, this stochastic acceleration appears to be very efficient. The high levels of compressional fluctuations observed in the heliosheath (Ness et al., this volume) support this view.

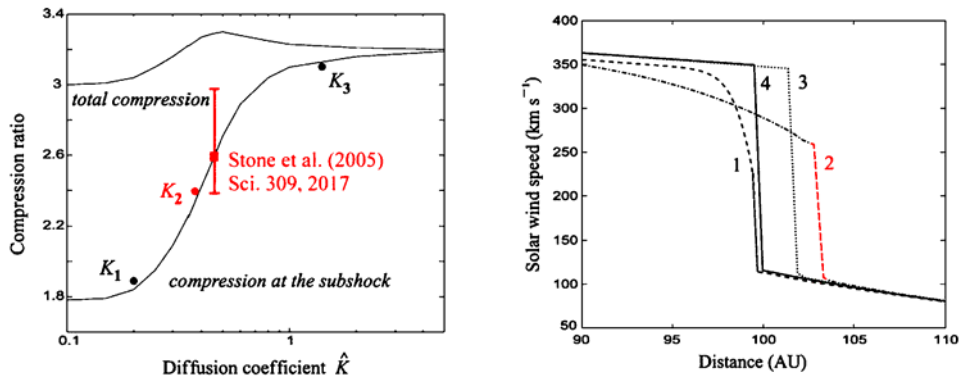


Figure 7.13: *Left*: Reduction of the solar wind termination shock compression ratio. *Right*: Shape of the precursor to be compared to the data in Figure 7.14 (Alexashov et al., 2004).

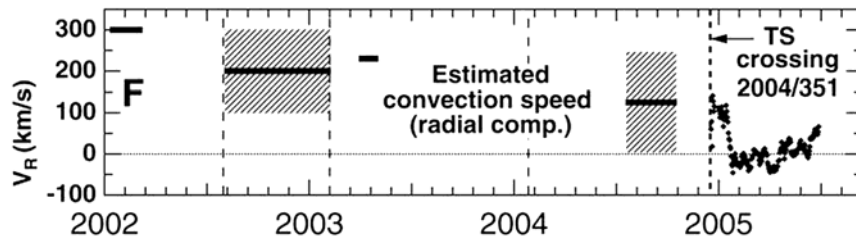


Figure 7.14: Observed slow-down of the solar wind upstream of the termination shock (Decker et al., 2005).

The data seem to support the idea that the solar wind termination shock is a cosmic-ray-mediated shock. Figure 7.13 shows the modelled reduction in the compression ratio of the solar wind termination subshock, in particular for the parallel mean free path denoted by Index 2 that corresponds to the model of the evolution of solar wind turbulence and the observed increase in turbulence at the shock (Figure 7.5). Figure 7.14 shows the slow-down of the solar wind observed by Voyager 1. The error bars are large because the plasma instrument onboard Voyager 1 is not operating anymore, so that the solar wind velocity has to be derived from anisotropies in the energetic particle flux measured by LECP. Although the uncertainties are large, the solar wind seems to be slowed down much below the speed of about 250–300 km/s , which corresponds to the maximum slow-down due to the mass loading of interstellar pick-up protons in the outer heliosphere. Therefore, it seems likely that the solar wind termination shock is cosmic-ray-mediated by the TSP/ACR population. However, as is visible from Figure 7.6, the energetic particle pressure gradient in the upstream solar wind plasma is not in the form of a smooth precursor, but rather spiky and intermittent.

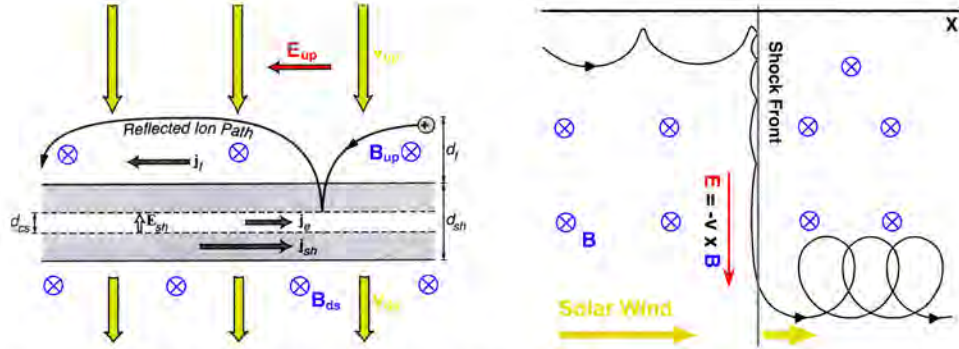


Figure 7.15: *Left*: Simplified structure of a perpendicular shock: Protons penetrate into the downstream plasma with the scale size of their gyroradius, while electrons are ‘stopped’ within an electron gyroradius. This charge separation causes a cross-shock electric field E_{sh} over the ramp scale size of order d_{cs} . The cross-shock potential $e\phi = eE_{sh}d_{cs}$ is of the order of the upstream proton energy, i.e. the kinetic bulk plasma energy. The jump in the tangential component of the magnetic field $[B_t] = B_{ds} - B_{up} > 0$ causes a current $j_{sh} = [B_t] / (\mu_0 d_{cs})$, according to $\mu_0 \mathbf{j} = \nabla \times \mathbf{B}$. The shock current j_{sh} increases the downstream magnetic field, and consequently is responsible for a downstream ‘overshoot’ of the magnetic field. This overshoot is increased by an $\mathbf{E}_{sh} \times \mathbf{B}$ drift current \mathbf{j}_e of the electrons in the cross-shock potential. The effect of reflected ions is particularly strong for the termination shock because a large fraction of pick-up ions with their shell-like velocity distribution (Geiss et al., this volume) is reflected in the cross-shock electric field and the pick-up ion pressure near the termination shock is comparable to the bulk plasma pressure. The reflected ions form an upstream current \mathbf{j}_r that causes a ‘foot’ in the upstream magnetic field (adapted from Baumjohann and Treumann, 1996, p. 183). *Right*: The specularly reflected ions are also accelerated in the upstream convective electric field \mathbf{E}_{up} until they have sufficient energy to cross the shock potential $\phi = E_{sh}d_{cs}$. These ions, accelerated by ‘shock surfing’ may surpass the injection threshold for first-order Fermi acceleration (from Möbius and Kallenbach, 2005).

7.6 The injection problem: shock surfing vs. stochastic acceleration

Besides the scale length of the ACR pressure, the scale length of the termination shock ramp is an important characteristic size that has an influence on suprathermal particle populations. If the scale size of the shock ramp of a quasi-perpendicular shock, d_{cs} , is of the order of the electron inertial length, $d_{cs} \approx L_e = c/\omega_{pe}$, the pick-up ions may undergo acceleration in the convective electric field \mathbf{E}_{up} (Figure 7.15) of the shock front during multiple reflections at the electric cross-shock potential $\phi = E_{sh}d_{cs}$ (le Roux et al., 2000). This kind of acceleration is most efficient when the pickup ions are trapped at the shock between the electrostatic cross-shock potential $\phi = E_{sh}d_{cs}$ and the upstream Lorentz force (shock surfing; Sagdeev, 1966; Zank et al., 1996b; Lee et al., 1996). Trapping occurs if (1) the particles’ incident normal velocity v_x satisfies the condition

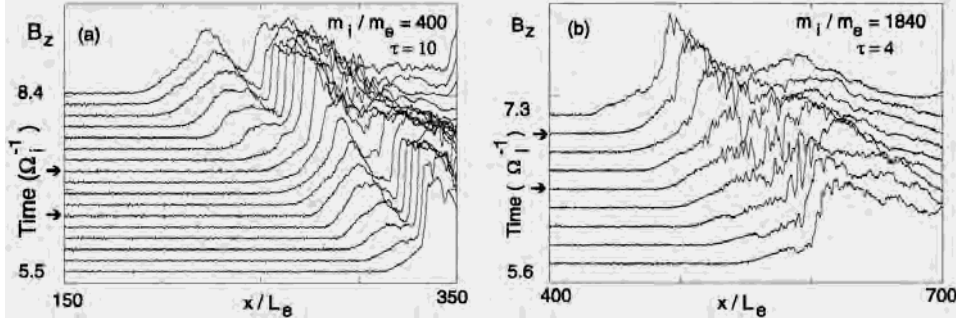


Figure 7.16: Reformation of a quasi-perpendicular shock (Scholer et al., 2003). Present computer resources prohibit a simulation with a realistic mass ratio m_i/m_e and at the same time a value of $\tau = (\omega_{pe}/\Omega_{ce})^2$ appropriate for the solar wind. However, from independent variations of both parameters, the structure of the termination shock has been inferred, assuming a shock normal angle to the downstream magnetic field of $\theta_{Bn} = 87^\circ$.

($m/2)v_x^2 \ll e\phi$, where m is the particles' mass, and e the electron charge, and (2) the Lorentz force is smaller than the force exerted by the electrostatic potential $e\phi$, i.e., $ev_y B < e\phi/d_{cs}$, where B is the magnetic field magnitude in the shock ramp. Thus, the maximum energy a particle can reach by shock surfing is inversely proportional to the square of the cross-shock potential length scale d_{cs} . Assuming that the cross-shock potential is of the order of the upstream bulk energy per charge, and that d_{cs} is of the order of the electron inertial length L_e , the maximum pickup ion energy is close to about 1 MeV/amu for ions of any atomic mass A or atomic charge Q . This is sufficient to overcome the injection threshold for first-order Fermi acceleration (Figure 7.8).

However, the typical shock ramp scale size may be much larger, of the order of the ion (proton) inertial length $L_p = L_e \sqrt{m_p/m_e}$ or of the order of the gyroradius (Larmor radius). The latter scale size would be plausible from Figure 7.15. The shock ramp can be as short as the electron inertial length, if the shock wave is similar to a damped solitary magnetosonic wave (Tidman and Krall, 1971).

Scholer et al. (2003) have performed one-dimensional (1-D) full particle simulations of almost perpendicular supercritical collisionless shocks. The ratio of electron plasma frequency ω_{pe} to gyrofrequency Ω_{ce} , the ion-to-electron mass ratio, and the ion and electron β (β = plasma to magnetic field pressure) have been varied. Due to the accumulation of specularly reflected ions upstream of the shock, ramp shocks can reform on time scales of the gyroperiod in the ramp magnetic field (Figure 7.16).

Figure 7.17 demonstrates the process by which reformation occurs. It shows a $v_{ix}x$ phase space plot for $\beta_i = 0.1$ at a specific time and the respective magnetic field profile. The large velocity difference between the cold incoming solar wind distribution and the cold specularly reflected ions results in a large-scale vortex between the ramp and the position upstream where the reflected ions are turned around perpendicular to the shock normal and to the magnetic field, and accumu-

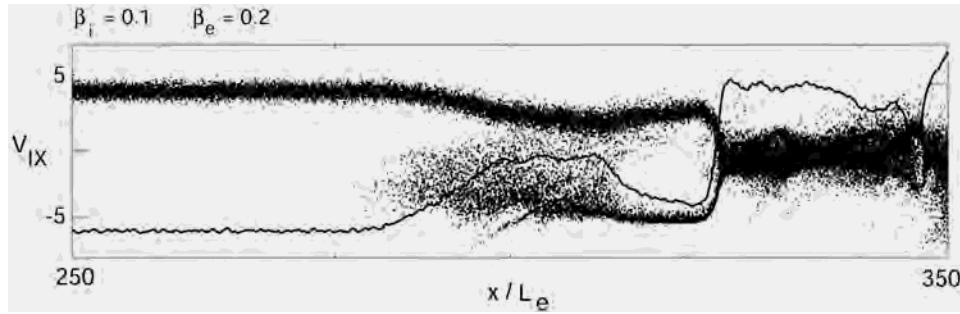


Figure 7.17: $v_{ix} - x$ phase space plot and superimposed magnetic field profile at a specific time (Scholer et al., 2003).

late. Since B/n is essentially constant in a compressible plasma, this results in an upstream magnetic field hump. The solar wind is slowed down, and the solar wind density increases, causing a further magnetic field increase. Eventually the hump takes over the role of the reformed shock. This behaviour of the ion phase space density is typical for all reformation cycles.

Self-reformation is not only a low ω_{pe}/Ω_{ce} process, but occurs also in $(\omega_{pe}/\Omega_{ce})^2 \gg 1$, low- β simulations. Self-reformation also occurs in low ion β runs with an ion to electron mass ratio $m_i/m_e = 1840$, so that it may actually occur at the solar wind termination shock. However, in the realistic mass ratio runs, an electromagnetic instability is excited in the foot of the shock, and the shock profile is considerably changed compared to lower mass ratio runs. Linear analysis based on three-fluid theory with incident ions, reflected ions, and electrons (Matsukiyo and Scholer, 2003) indicates that the instability is a modified two-stream instability between the decelerated solar wind electrons and the solar wind ions on the whistler mode branch. If the waves generated by this instability are sufficiently strong to trap pick-up ions, it may be the instability that causes the self-reformation.

In the reforming shock, part of the potential drop occurs at times across the foot, and part of the potential ($\sim 40\%$) occurs over a few ($\sim 4L_e$) electron inertial lengths in the steepened-up ramp. Self-reformation is a low ion β process and disappears for a Mach 4.5 shock at/or above an ion $\beta_i \sim 0.4$. The ion thermal velocity has to be an order of magnitude smaller than the shock velocity in order for reformation to occur. Scholer et al. (2003) conclude that according to these simulations only part of the potential drop occurs for relatively short times over a few electron inertial lengths L_e , and that, therefore, coherent shock surfing is not an efficient acceleration mechanism for pickup ions at the low β_i heliospheric termination shock.

Nonetheless, the electric shock potential may have important consequences for Anomalous Cosmic Ray and Termination Shock Energetic Particles (ACRs and TSPs). Possibly, these abundances can be explained by the following scenario: (1) TSPs are ions that are multiply reflected at the shock potential and injected into first-order Fermi acceleration, which has an injection threshold much lower than often assumed (Figure 7.8). The TSPs do not undergo mass-per-charge (A/Q) fractionation because shock surfing is a process independent of A/Q . (2) ACRs

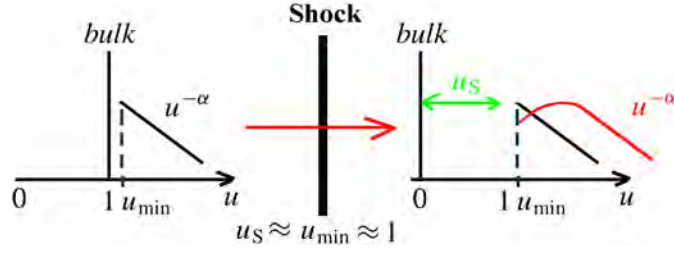


Figure 7.18: Schematic showing the characteristics of the transmission of power-law suprathermal tails through a shock potential.

are suprathermal ions directly transmitted through the electric potential of the termination shock, but not returned to the shock for first-order Fermi acceleration. These ions undergo stochastic acceleration in the heliosheath. The transmission through the termination shock potential prefers high A/Q species in concordance with ACR abundances. (3) A fraction of the reflected ions are thermalized into the bulk plasma of the heliosheath. Low A/Q species are preferentially thermalized. This scenario would match observations. For instance, the H/He ratio is about 10 for TSPs and about 5 for ACRs (Stone et al., 2005).

This ‘transmission’ scenario is quite simple, but can be explained in some more detail as follows: Three populations approach the termination shock from the upstream solar wind: (1) the bulk solar wind ions idealized as a pencil beam $f_{\text{bulk}} \propto \delta(u-1, \mu-1)$, (2) the freshly ionized pick-up ions in a shell distribution $q(u) \propto \delta(u-1)$, and (3) the suprathermal tails $f_{\text{ST}} \propto u^{-\alpha}$ for $u > u_{\text{min}}$. The suprathermal tails at the termination shock presumably reach down to almost $u_{\text{min}} \approx 1$ ($u = v/V_{\text{up}}$ with V_{up} the upstream solar wind speed) because the speeds of the waves causing these tails are much smaller than the speed $U_{\text{up}} = 1$ of the supersonic bulk solar wind. Population (2) is presumably negligible at the termination shock (Kallenbach et al., 2005). In a very idealized picture, the cross-shock potential is characterized by $u_S = V_S/V_{\text{up}} \approx 1$, which stops the bulk protons to zero speed and conserves the number of suprathermal ions at $u > u_{\text{min}}$. Of course, in reality u_S is less than unity because the downstream plasma does not have zero speed.

We define a normalized transmission function $T_{\text{S};\mathcal{R}}$ for the suprathermal tails, which yields the downstream distribution function when multiplied with the upstream distribution function. The upstream distribution function is assumed to be a power-law above the minimum speed u_{min} with the same spectral index α as upstream. The data of Figure 7.5 suggest that this is a valid approach. Therefore, the normalized transmission function $T_{\text{S};\mathcal{R}}$ for the suprathermal tails at speeds $u > u_{\text{min}}$ is (see Figure 7.18 for an illustration):

$$\int_{u_{\text{min}}}^{\infty} u^{-\alpha+2} du = T_{\text{n};\mathcal{R}} \int_{\frac{u_S}{\sqrt{\mathcal{R}}}}^{\infty} \left(1 - \frac{u_S^2}{\mathcal{R}u^2}\right) u^{-\alpha+2} du$$

$$\Rightarrow T_{\text{n};\mathcal{R}} = \frac{\alpha-1}{2} \left(\frac{u_S}{\sqrt{\mathcal{R}}u_{\text{min}}}\right)^{\alpha-3} ; \quad T_{\text{S};\mathcal{R}} = T_{\text{n};\mathcal{R}} \left(1 - \frac{u_S^2}{\mathcal{R}u^2}\right). \quad (7.10)$$

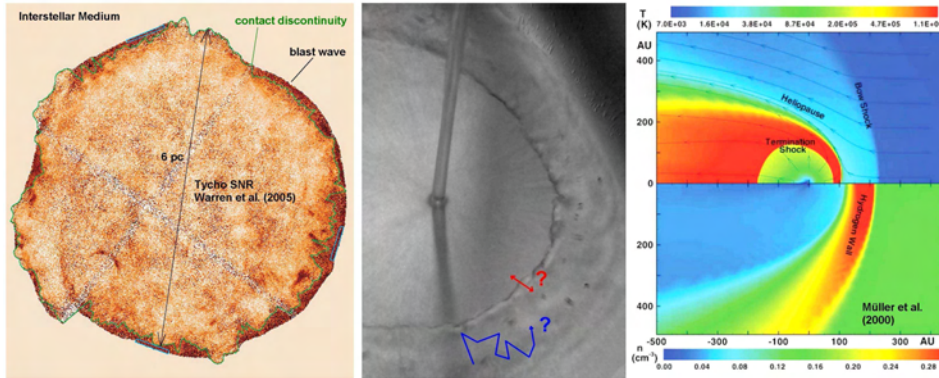


Figure 7.19: Comparison of the Tycho supernova bubble with the heliosphere.

The normalizing factor $T_{n;\mathcal{R}}$ indicates the increase in the phase space density at high speeds downstream, and hence yields the availability of suprathermal ions in the heliosheath for further stochastic acceleration. If further stochastic acceleration occurs by compressional fluctuations, no more A/Q fractionation occurs, and the ACR abundances are given by the transmission factor $T_{n;\mathcal{R}}$. For the typical tails with $\alpha \approx 5$, the fractionation pattern is mass-proportional for singly charged pickup ions. For larger α , the fractionation is stronger.

7.7 Conclusions

Turbulence and ion acceleration are intimately linked processes of the outer heliosphere. The analysis of this article supports the idea that stochastic acceleration in compressional fluctuations in the heliosheath is a process that can compete with first-order Fermi acceleration at the solar wind termination shock. A viable explanation for the composition of Termination Shock Energetic Particles (TSPs) and Anomalous Cosmic Rays (ACRs) is that TSPs are particles which are reflected as slightly suprathermal ions at the electric cross-shock potential of the solar wind termination shock (TS) and subsequently accelerated by the first-order Fermi process, while ACRs are particles transmitted as slightly suprathermal ions through the electric cross-shock potential of the TS and subsequently stochastically accelerated in the compressional fluctuations of the heliosheath. Probably, the two processes of first-order Fermi acceleration and second-order Fermi acceleration are intertwined. Particles that are stochastically accelerated in the heliosheath may eventually reach an energy which gives them a sufficiently large mean free path to cross the TS again to participate in first-order Fermi acceleration.

Lessons may be learned from the heliosphere for galactic acceleration processes. Second-order Fermi acceleration may also be responsible for the energization of the Galactic Cosmic Rays (GCRs). Warren et al. (2005) have observed that the turbulence region downstream of the blast wave of the Tycho supernova is thinner than magnetohydrodynamic models predict (Figure 7.19). This may be analogous with the reduced size of the heliosheath due to the ACR pressure there. As the

sum of the ACR pressure and the heliosheath bulk pressure balances the pressure of the interstellar medium, the heliosheath bulk pressure is reduced in the presence of the ACRs and the size of the heliosheath is consequently reduced.

This has been taken as an argument for the presence of GCRs in the region between the blast wave and the contact discontinuity of the bubble of the Tycho supernova. In fact, it has been taken as evidence that a supernova shock wave accelerates the GCRs. This result may have to be verified. It may actually be the turbulence downstream of the supernova shock that accelerates the GCRs.

Appendix

7.A Diffusion of charged particles

Diffusion parameters are usually derived in the literature with significant mathematical effort. In principle, they easily trace back to the Vlasov-Maxwell equation. The Vlasov-Maxwell equation states that the total variation of the distribution function of a suprathermal particle species s is extremal, which leads to

$$(\partial_t + \mathbf{v} \cdot \nabla) f_s + \nabla_{\mathbf{v}} f_s \cdot \dot{\mathbf{v}} = 0. \quad (7.11)$$

Usually the distinction is made between diffusion in non-compressional and diffusion in compressional fluctuations. In the first case the plasma is treated as a plasma with uniform bulk speed containing Alfvénic magnetic field fluctuations with wave amplitudes $\delta\mathbf{B}$ and $\delta\mathbf{E}$ perpendicular to the ambient magnetic field, $\delta\mathbf{E} \perp \mathbf{B}_0$, $\delta\mathbf{B} \perp \mathbf{B}_0$, and $\delta\mathbf{E} \perp \delta\mathbf{B}$. In the second case, as a consequence of compression, there are fluctuations $\delta\mathbf{U} \parallel \mathbf{B}_0$. It is convenient to choose a coordinate system in which the mean plasma velocity is zero, $\langle \mathbf{U} \rangle = 0$. The particle velocity can then be split into two parts $\mathbf{v} = \mathbf{v}' + \delta\mathbf{U}$, where it is convenient to drop the prime for the particle velocity in the plasma frame. The Vlasov-Maxwell equation then reads

$$(\partial_t + \mathbf{v} \cdot \nabla + \delta\mathbf{U} \cdot \nabla) f_s + \nabla_{\mathbf{v}} f_s \cdot (\dot{\mathbf{v}} + \delta\dot{\mathbf{U}}) = 0. \quad (7.12)$$

7.A.1 Diffusion in non-compressional magnetic field fluctuations in slab geometry

We assume a homogeneous plasma with $\mathbf{E}_0 = 0$, $\delta\mathbf{U} = 0$, and an ambient magnetic field \mathbf{B}_0 . To the equilibrium distribution of the suprathermal species s with charge-to-mass ratio $\eta_s := q_s/m_s$, determined by

$$\partial_t f_s + (\mathbf{v} \cdot \nabla) f_s + \eta_s (\mathbf{v} \times \mathbf{B}_0) \cdot \nabla_{\mathbf{v}} f_s = 0, \quad (7.13)$$

we add small fluctuating fields $\delta\mathbf{E}$ and $\delta\mathbf{B}$, and a small deviation δf_s of the distribution function. Adding these terms to the above equation yields to first order:

$$\begin{aligned} \partial_t \delta f_s + (\mathbf{v} \cdot \nabla) \delta f_s + \eta_s (\delta\mathbf{E} + \mathbf{v} \times \delta\mathbf{B}) \cdot \nabla_{\mathbf{v}} f_s + \eta_s (\mathbf{v} \times \mathbf{B}_0) \cdot \nabla_{\mathbf{v}} \delta f_s &= 0 \\ \Rightarrow (-i\omega + i\mathbf{v} \cdot \mathbf{k}) \delta f_s + \eta_s (\delta\mathbf{E} + \mathbf{v} \times \delta\mathbf{B}) \cdot \nabla_{\mathbf{v}} f_s &= 0 \\ \Rightarrow \delta f_s = \eta_s \frac{\delta\mathbf{E} + \mathbf{v} \times \delta\mathbf{B}}{i(\omega - \mathbf{v} \cdot \mathbf{k})} \cdot \nabla_{\mathbf{v}} f_s \Rightarrow \nabla_{\mathbf{v}} \delta f_s = \eta_s \nabla_{\mathbf{v}} \left[\frac{\delta\mathbf{E} + \mathbf{v} \times \delta\mathbf{B}}{i(\omega - \mathbf{v} \cdot \mathbf{k})} \cdot \nabla_{\mathbf{v}} f_s \right]. \end{aligned} \quad (7.14)$$

The last term of the first line is zero because $\nabla_{\mathbf{v}} \perp \mathbf{v}$. Adding $\nabla_{\mathbf{v}} \delta f_s$ to ∇f_s in the above first-order Vlasov-Maxwell equation and averaging over the fluctuation scales, one identifies the second-order macroscopic term

$$\eta_s \langle |(\delta\mathbf{E} + \mathbf{v} \times \delta\mathbf{B}) \cdot \nabla_{\mathbf{v}} \delta f_s| \rangle = \eta_s^2 \left\langle \left| (\delta\mathbf{E} + \mathbf{v} \times \delta\mathbf{B}) \cdot \nabla_{\mathbf{v}} \left[\frac{\delta\mathbf{E} + \mathbf{v} \times \delta\mathbf{B}}{(\mathbf{v} \cdot \mathbf{k} - \omega)} \cdot \nabla_{\mathbf{v}} f_s \right] \right| \right\rangle. \quad (7.15)$$

We transform the above term in such a way that it describes a diffusion equation. With $\mathbf{a} := \eta_s^2 (\delta \mathbf{E} + \mathbf{v} \times \delta \mathbf{B})$, $\mathbf{b} := \nabla_{\mathbf{v}} (\mathbf{c} \cdot \mathbf{d})$, $\mathbf{c} := (\delta \mathbf{E} + \mathbf{v} \times \delta \mathbf{B}) (\mathbf{k} \cdot \mathbf{v} - \omega)^{-1}$, and $\mathbf{d} := \nabla_{\mathbf{v}} f_s$ we obtain

$$\begin{aligned} \langle \mathbf{a} \cdot \mathbf{b} \rangle &= \left\langle \sum_{i=1}^3 a_i b_i \right\rangle = \left\langle \sum_{i,j} a_i \frac{\partial (c_j d_j)}{\partial v_i} \right\rangle = \left\langle \sum_{i,j} \frac{\partial (a_i c_j d_j)}{\partial v_i} - \sum_{i,j} c_j d_j \frac{\partial a_i}{\partial v_i} \right\rangle \\ &= \left\langle \nabla_{\mathbf{v}} \cdot \tilde{D} \nabla_{\mathbf{v}} f_s \right\rangle; \quad \tilde{D} = \eta_s^2 \left\langle \left| \frac{(\delta \mathbf{E} + \mathbf{v} \times \delta \mathbf{B}) \otimes (\delta \mathbf{E} + \mathbf{v} \times \delta \mathbf{B})}{(\mathbf{k} \cdot \mathbf{v} - \omega)} \right| \right\rangle. \end{aligned} \quad (7.16)$$

The last step follows because $\nabla_{\mathbf{v}} \cdot \mathbf{a} = 0$ as the fields do not depend on the velocity \mathbf{v} . Also, we have taken the term $\nabla_{\mathbf{v}} f_s$ out of the averaging parenthesis because this is the mean distribution function describing the evolution on space and time scales larger than the fluctuation scales. The tensor \tilde{D} is the general form of a diffusion tensor, with which the stochastic motion of the charged minority particles in the plasma is described. Two parameters are relevant: (1) the power, which is in the plasma waves, and (2) the resonance condition that is applied to describe the wave-particle interaction between ions of species s and the waves.

We evaluate the direct product $\tilde{A} = (\delta \mathbf{E} + \mathbf{v} \times \delta \mathbf{B}) \otimes (\delta \mathbf{E} + \mathbf{v} \times \delta \mathbf{B})$ for ‘slab’ geometry turbulence which propagates gyrotropically parallel to the ambient magnetic field, $\mathbf{k} \parallel \mathbf{B}_0$. As $\nabla \cdot \mathbf{B} = 0$ we have $\delta \mathbf{B} \perp \mathbf{B}_0$. Furthermore, for MHD-modes, we have $\nabla \times \delta \mathbf{E} = -\delta \dot{\mathbf{B}}$ or in Fourier components $\delta \mathbf{E} = -\hat{\mathbf{k}} \times \delta \mathbf{B} \omega / k = -\hat{\mathbf{k}} \times \delta \mathbf{B} V_{\text{ph}}$. This means that the electric fluctuation amplitude is $\delta \mathbf{E} = -\mathbf{V}_{\text{ph}} \times \delta \mathbf{B}$, i.e. the negative cross product of the phase velocity with the magnetic fluctuation amplitude. In other words, the electric field amplitude is zero in the wave frame. We take $\delta \mathbf{B} = \delta B \mathbf{e}_x$ and define $v'_{\parallel} = v_{\parallel} - V_{\text{ph}}$. This yields

$$\begin{aligned} (\mathbf{v} - \mathbf{V}_{\text{ph}}) \times \delta \mathbf{B} &= v'_{\parallel} \delta B \mathbf{e}_y - v_{\perp} \delta B \sin \phi \mathbf{e}_z \\ &= \delta B \left[v'_{\parallel} \sin \phi (\mathbf{e}_r \sin \theta + \mathbf{e}_{\theta} \cos \theta) + v'_{\parallel} \mathbf{e}_{\phi} \cos \phi - v_{\perp} \sin \phi (\mathbf{e}_r \cos \theta - \mathbf{e}_{\theta} \sin \theta) \right] \\ &= \delta B \left[\mathbf{e}_r \sin \phi (v'_{\parallel} \sin \theta - v_{\perp} \cos \theta) + \mathbf{e}_{\theta} \sin \phi (v'_{\parallel} \cos \theta + v_{\perp} \sin \theta) + \mathbf{e}_{\phi} v'_{\parallel} \cos \phi \right]. \end{aligned} \quad (7.17)$$

The angle θ is the pitch angle, and the angle ϕ is the generally time-varying angle between the magnetic fluctuation amplitude $\delta B \mathbf{e}_x$ and the perpendicular velocity vector \mathbf{v}_{\perp} . We will see that we can drop the term $\mathbf{e}_{\phi} v'_{\parallel} \delta B \cos \phi$ because we derive the result for a gyrotropic situation. Because of

$$\begin{aligned} v'_{\parallel} \sin \theta - v_{\perp} \cos \theta &= -V_{\text{ph}} \sin \theta = -V_{\text{ph}} \sqrt{1 - \mu^2}, \\ v'_{\parallel} \cos \theta + v_{\perp} \sin \theta &= v - \mu V_{\text{ph}}, \quad \mu = \cos \theta, \end{aligned} \quad (7.18)$$

and averaging over $\sin^2 \phi$, we get

$$\begin{aligned} \tilde{A} &= \frac{\delta B^2}{2} \begin{pmatrix} -V_{\text{ph}} \sqrt{1 - \mu^2} \\ v - \mu V_{\text{ph}} \\ 0 \end{pmatrix} \otimes \begin{pmatrix} -V_{\text{ph}} \sqrt{1 - \mu^2} \\ v - \mu V_{\text{ph}} \\ 0 \end{pmatrix} \\ &= \frac{\delta B^2}{2} \begin{pmatrix} V_{\text{ph}}^2 (1 - \mu^2) & V_{\text{ph}} \sqrt{1 - \mu^2} (\mu V_{\text{ph}} - v) & \dots \\ V_{\text{ph}} \sqrt{1 - \mu^2} (\mu V_{\text{ph}} - v) & (v - \mu V_{\text{ph}})^2 & \dots \\ \dots & \dots & \dots \end{pmatrix}. \end{aligned} \quad (7.19)$$

If this tensor \tilde{A} is multiplied with the velocity gradient of a gyrotropic distribution $\nabla_{\mathbf{v}}f = (\partial_v f, \partial_\theta f/v, 0)$, then we get a vector \mathbf{A} :

$$\mathbf{A} = \frac{\delta B^2}{2} \begin{pmatrix} V_{\text{ph}}^2 (1 - \mu^2) \partial f / \partial v - V_{\text{ph}} \sqrt{1 - \mu^2} (1 - \mu V_{\text{ph}}/v) \partial f / \partial \theta \\ -V_{\text{ph}} \sqrt{1 - \mu^2} (v - \mu V_{\text{ph}}) \partial f / \partial v + v (1 - \mu V_{\text{ph}}/v) \partial f / \partial \theta \\ 0 \end{pmatrix}. \quad (7.20)$$

This vector's divergence in spherical coordinates divided by $\mathcal{R} = (\mathbf{k} \cdot \mathbf{v} - \omega)$ is

$$\begin{aligned} \frac{1}{v^2} \frac{\partial}{\partial v} (v^2 A_r) + \frac{1}{v \sin \theta} \frac{\partial}{\partial \theta} (\sin \theta A_\theta) &= \frac{1}{v^2} \frac{\partial}{\partial v} \left[v^2 V_{\text{ph}}^2 (1 - \mu^2) \frac{\delta B^2}{2\mathcal{R}} \frac{\partial f}{\partial v} \right] \\ &+ \frac{1}{v^2} \frac{\partial}{\partial v} \left[v^2 \frac{\delta B^2}{2\mathcal{R}} V_{\text{ph}} (1 - \mu^2) \left(1 - \frac{\mu V_{\text{ph}}}{v} \right) \frac{\partial f}{\partial \mu} \right] \\ &+ \frac{1}{v} \frac{\partial}{\partial \mu} \left[\frac{\delta B^2}{2\mathcal{R}} V_{\text{ph}} (1 - \mu^2) \left(1 - \frac{\mu V_{\text{ph}}}{v} \right) \frac{\partial f}{\partial v} \right] \\ &+ \frac{\partial}{\partial \mu} \left[\frac{\delta B^2}{2\mathcal{R}} (1 - \mu^2) \left(1 - \frac{\mu V_{\text{ph}}}{v} \right)^2 \frac{\partial f}{\partial \mu} \right]. \end{aligned} \quad (7.21)$$

Now we have to take the average of these expressions, which is equivalent to the integration of $\delta \tilde{B}^2(k)/\mathcal{R}$ over dk . For a slab geometry \mathbf{k} -space is only one-dimensional. Only the gyro-resonant interaction is taken into account, so that the integration is equivalent to a multiplication with $k_r^\pm = (\omega \pm \Omega)/(v\mu)$ of the value of the function at k_r^\pm . Equation (7.15) can now be written as

$$\begin{aligned} \frac{\partial f_s}{\partial t} &= \frac{\partial}{\partial \mu} \left(D_{\mu\mu} \frac{\partial f}{\partial \mu} \right) + \frac{\partial}{\partial \mu} \left(D_{\mu v} \frac{\partial f}{\partial v} \right) + \frac{1}{v^2} \frac{\partial}{\partial v} \left(v^2 D_{v\mu} \frac{\partial f}{\partial \mu} \right) + \frac{1}{v^2} \frac{\partial}{\partial v} \left(v^2 D_{vv} \frac{\partial f}{\partial v} \right) \\ D_{\mu\mu} &= \sum_{\pm} \frac{\Omega^2}{2} \left(1 - \frac{\mu V_{\text{ph}}}{v} \right)^2 \frac{(1 - \mu^2)}{v\mu - V_{\text{ph}}} \frac{\delta \tilde{B}^2(k_r^\pm)}{B_0^2} \\ D_{\mu v} &= D_{v\mu} = \sum_{\pm} \frac{\Omega^2}{2} \frac{V_{\text{ph}}}{v\mu - V_{\text{ph}}} \left(1 - \frac{\mu V_{\text{ph}}}{v} \right) (1 - \mu^2) \frac{\delta \tilde{B}^2(k_r^\pm)}{B_0^2} \\ D_{vv} &= \sum_{\pm} \frac{\Omega^2}{2} \frac{V_{\text{ph}}^2}{v\mu - V_{\text{ph}}} (1 - \mu^2) \frac{\delta \tilde{B}^2(k_r^\pm)}{B_0^2}. \end{aligned} \quad (7.22)$$

These are the most often used diffusion parameters which are found in the most recent literature (Isenberg et al. , 2003). While they give a useful description of pitch-angle scattering or parallel mean free paths, respectively, in the supersonic solar wind plasma, they do not necessarily reflect the proper description of momentum diffusion and perpendicular diffusion.

7.A.2 Momentum diffusion in compressional fluctuations

We go back to Equation (7.12), but add compressional fluctuations $\delta \mathbf{U} \parallel \mathbf{B}_0$:

$$(\partial_t + \mathbf{v} \cdot \nabla + \delta \mathbf{U} \cdot \nabla) f_s + \nabla_{\mathbf{v}} f_s \cdot (\dot{\mathbf{v}} + \delta \dot{\mathbf{U}}) = 0. \quad (7.23)$$

The compressional fluctuations have much larger temporal and spatial scale than the magnetic fluctuations in a slab geometry. The term $\dot{\mathbf{v}}$ leads to the diffusion parameters treated above. The term $\delta\dot{\mathbf{U}}$, however, yields additional momentum diffusion in analogy with \tilde{D} in Equation (7.16):

$$\tilde{D} = \left\langle \frac{\delta\dot{\mathbf{U}} \otimes \delta\dot{\mathbf{U}}}{[\mathbf{k} \cdot (\mathbf{v} + \delta\mathbf{U}) - \omega]} \right\rangle \approx \left\langle \frac{\delta\dot{\mathbf{U}} \otimes \delta\dot{\mathbf{U}}}{\mathbf{k} \cdot \delta\mathbf{U}} \right\rangle \quad \text{if } \lambda_{\parallel} \ll L_{\text{cor}}. \quad (7.24)$$

The latter approximation is a substantial shortcut for all the mathematics formulated in Bykov and Toptygin (1993) for the case that the mean free path for pitch-angle scattering is small compared to the correlation length of the large-scale compressional fluctuations, $\lambda_{\parallel} \ll L_{\text{cor}}$. It takes $\langle \mathbf{k} \cdot \mathbf{v} \rangle = \langle kv\mu \rangle$ as a small number because the pitch angle cosine μ changes rapidly over the trajectory of a charged particle. The interaction between waves and charged particles is dominated by $kv\mu - \omega \approx 0$. This leaves the above term. We further evaluate

$$\delta\dot{\mathbf{U}} \otimes \delta\dot{\mathbf{U}} \approx [\partial_t + (\delta\mathbf{U} + \mathbf{v}) \cdot \nabla] \delta\mathbf{U} \otimes [\partial_t + (\delta\mathbf{U} + \mathbf{v}) \cdot \nabla] \delta\mathbf{U}. \quad (7.25)$$

We neglect $\delta\mathbf{U} \cdot \nabla$ and ∂_t with respect to $\mathbf{v} \cdot \nabla$. Then we express $\delta\mathbf{U} = \mathbf{e}_z \delta U = \delta U (\mathbf{e}_r \cos \theta - \mathbf{e}_\theta \sin \theta)$ in spherical coordinates. The ∇ -operator only acts along the direction of the ambient magnetic field \mathbf{B}_0 , i.e. along the z -axis on $\delta\mathbf{U}$. Therefore, $\mathbf{v} \cdot \nabla = v\mu\partial_z$. The tensor \tilde{A} in analogy with Equation (7.19) is

$$\begin{aligned} \tilde{A} &= v^2 \mu^2 (\partial_z U)^2 \begin{pmatrix} \mu & & \\ -\sqrt{1-\mu^2} & & \\ 0 & & \end{pmatrix} \otimes \begin{pmatrix} \mu & & \\ -\sqrt{1-\mu^2} & & \\ 0 & & \end{pmatrix} \\ &= v^2 \mu^2 (\partial_z U)^2 \begin{pmatrix} \mu^2 & -\mu\sqrt{1-\mu^2} & \dots \\ -\mu\sqrt{1-\mu^2} & 1-\mu^2 & \dots \\ \dots & \dots & \dots \end{pmatrix}. \end{aligned} \quad (7.26)$$

The vector \mathbf{A} in analogy with Equation (7.20) is

$$\mathbf{A} = \mu^2 v^2 (\partial_z U)^2 \begin{pmatrix} \mu^2 \partial f / \partial v + \mu (1 - \mu^2) v^{-1} \partial f / \partial \mu \\ -\mu \sqrt{1 - \mu^2} \partial f / \partial v - (1 - \mu^2)^{3/2} \partial f / \partial \mu \\ 0 \end{pmatrix}. \quad (7.27)$$

The diffusion parameters in analogy with Equation (7.22) are

$$\begin{aligned} D_{\mu\mu} &= \left\langle \mu^2 (1 - \mu^2)^2 (\partial_z U)^2 (\mathbf{k} \cdot \delta\mathbf{U})^{-1} \right\rangle \\ D_{\mu v} &= D_{v\mu} = v \left\langle \mu^3 (1 - \mu^2) (\partial_z U)^2 (\mathbf{k} \cdot \delta\mathbf{U})^{-1} \right\rangle \\ D_{vv} &= v^2 \left\langle \mu^4 (\partial_z U)^2 (\mathbf{k} \cdot \delta\mathbf{U})^{-1} \right\rangle \propto v^2 \langle \delta U^2 \rangle^{1/2} L_{\text{cor}}^{-1}. \end{aligned} \quad (7.28)$$

These momentum and spatial diffusion parameters correspond to those derived in more detail in Le Roux et al. (2005).

7.A.3 Spatial diffusion

The spatial diffusion along the ambient magnetic field is caused by *pitch-angle scattering* (parameter $D_{\mu\mu}$ in Equation 7.22). If there is a spatial gradient in the density of suprathermal ions along the ambient magnetic field, more ions are scattered in the direction of decreasing density rather than in the opposite direction. The spatial diffusion coefficient is calculated as

$$\frac{v\lambda_{\parallel}}{3} = \kappa_{\parallel} = v^2 \int_0^1 \frac{\mu d\mu}{2} \int_0^{\mu} \frac{1 - \mu'^2}{D_{\mu'\mu'}} d\mu' . \quad (7.29)$$

It is plausible that the parallel mean free path λ_{\parallel} scales inversely with the rate of *pitch-angle scattering*. Large $D_{\mu\mu}$ means a large frequency of direction changes of order π . The ion rapidly changes direction from “backward” to “forward” motion and does not get very far. At low scattering frequency, however, the ions move far along the magnetic field without distortion of their trajectory.

The double integral is explained as follows: $D_{\mu'\mu'}^{-1} = \tau_{\mu'}$ is the temporal expectation value for scattering in the pitch angle at pitch-angle cosine $\mu' = \cos \Psi'$ and has the dimension time / $\cos^2 \Psi$. The increase in the quadratic parallel velocity through a change $d\mu'$ is $v'^2 = v^2 (1 - \mu'^2) d\mu'$. The quadratic distance per time that an ion moves while scattering from $\mu = 0$ to $\mu \neq 0$ is given by the inner integral over $v'^2 \tau_{\mu'} d\mu'$. The statistics representing the fact that scattering not only occurs from smaller to larger μ , but also vice versa, is given by averaging over the half-sphere $0 < \mu < 1$.

In Equation (7.22) the coefficient $D_{\mu\mu}$ has been given as a function of the power spectral density of the magnetic fluctuations:

$$D_{\mu\mu} = \sum_{\pm} \frac{\Omega^2}{2} \left(1 - \frac{\mu V_{\text{ph}}}{v}\right)^2 \frac{(1 - \mu^2) \delta \tilde{B}^2(k_r^{\pm})}{v\mu - V_{\text{ph}}} \frac{1}{B_0^2} . \quad (7.30)$$

Therefore, the parallel mean free path is

$$\lambda_{\parallel}^{\pm} = \frac{3v^2}{16\Omega^2} P^{-1}(k_r^{\pm}) \quad \text{mit} \quad P(k_r^{\pm}) = \frac{\delta \tilde{B}^2(k_r^{\pm})}{B_0^2} . \quad (7.31)$$

In the literature one usually finds the version with the factor $3/(8\pi)$ instead of $3/16$. Figure 7.20 shows experimentally determined parallel mean free paths, which approximately match QLT. These mean free paths have been determined from a fit to measured turbulence levels upstream of an interplanetary shock and from the spatial gradients of suprathermal particle populations. The turbulence level varies because the energetic protons generate waves near the shock.

7.A.4 Derivation of the injection threshold

The derivation of Equation (7.6) is based on estimates for the streaming flux

$$\mathbf{S} = \tilde{\kappa} \nabla f - \mathbf{V} \frac{v}{3} \frac{\partial f}{\partial v} ; \quad \nabla \cdot \mathbf{S} = \nabla \cdot (\tilde{\kappa} \nabla f) - \frac{v}{3} \frac{\partial f}{\partial v} \nabla \cdot \mathbf{V} . \quad (7.32)$$

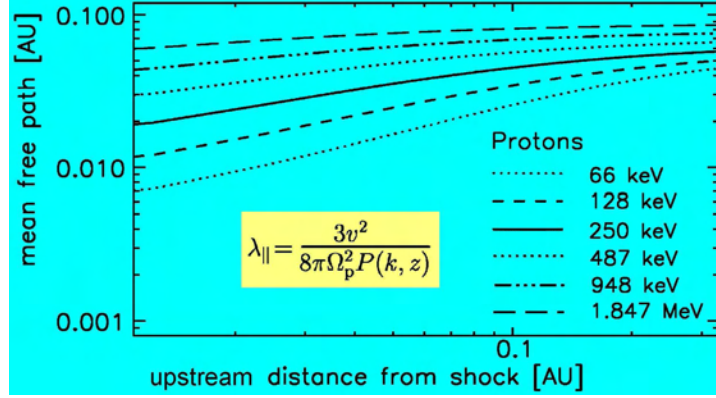


Figure 7.20: Experimentally determined mean free paths *upstream* of the strongest interplanetary shock of the Bastille Day event (Bamert et al., 2004).

The first term in the streaming flux is the anisotropic “diffusion speed” $\tilde{\kappa}\nabla f$ with

$$\tilde{\kappa} = \begin{pmatrix} \kappa_{\parallel} & 0 & 0 \\ 0 & \kappa_{\perp} & \kappa_A \\ 0 & -\kappa_A & \kappa_{\perp} \end{pmatrix};$$

$$\kappa_{\parallel} = \frac{1}{3}v\lambda_{\parallel}; \quad \frac{\kappa_{\perp}}{\kappa_{\parallel}} = \frac{r_g^2}{\lambda_{\parallel}^2} \frac{1}{1 + (r_g/\lambda_{\parallel})^2} \approx \frac{r_g^2}{\lambda_{\parallel}^2}; \quad \frac{\kappa_A}{\kappa_{\parallel}} = \frac{r_g}{\lambda_{\parallel}} \frac{1}{1 + (r_g/\lambda_{\parallel})^2} \approx \frac{r_g}{\lambda_{\parallel}}. \quad (7.33)$$

The parameter κ_{\perp} may become plausible with the following considerations: If we assume turbulence with correlation length $l_{c:A} \approx r_g$ and $\zeta_A = \langle \delta B_A^2 \rangle / B_0^2 \approx 1$, then the parallel mean free path λ_{\parallel} is of the order of the gyroradius r_g and parallel and perpendicular gyrations have about the same amplitude. The latter means $\lambda_{\parallel} \approx \lambda_{\perp}$, i.e. $\kappa_{\parallel} \approx \kappa_{\perp}$.

For decreasing turbulence amplitude, the parallel mean free path increases while the particle has difficulties in moving across the ambient magnetic field. For small ζ_A we have $\lambda_{\parallel} \gg r_g \gg \lambda_{\perp}$ with $\lambda_{\perp}\lambda_{\parallel} \approx r_g^2$. The parameter κ_A describes a superposition of gyration and scattering.

The term $(v/3)(\partial f/\partial v)\nabla \cdot \mathbf{V}$ can be understood as an expansion in orders of the speed $|\mathbf{V}|$ of the convective derivative of the distribution function $f(\mathbf{v} + \mathbf{V})$ in a medium streaming with velocity \mathbf{V} :

$$\langle (\mathbf{v} + \mathbf{V}) \cdot \nabla f(\mathbf{v} + \mathbf{V}) \rangle \approx \mathbf{V} \cdot \nabla f(\mathbf{v}) + \left\langle \mathbf{v} \cdot \nabla \left[\frac{\partial f(\mathbf{v})}{\partial \mathbf{v}} \cdot \mathbf{V} \right] \right\rangle. \quad (7.34)$$

The brackets mean directional averaging for nearly isotropic distributions. Taking the direction of the streaming velocity \mathbf{V} as the projection axis, the two scalar products lead to a term μ^2 , and averaging gives a factor of $1/3$.

The spatial diffusion speed $\tilde{\kappa}\nabla f$ increases with speed. At some injection threshold speed v_{inj} the downstream diffusion speed will balance the upstream convection speed. This means that the majority of particles are not just convected through the shock, but undergo diffusion, i.e. scattering back and forth across the shock.

The diffusion speed along the shock normal has to be evaluated for a planar shock. The diffusion tensor $\tilde{\kappa}$ refers to the reference system fixed to the ambient magnetic field. The transformation on the shock normal is performed by a rotation by the shock normal angle Ψ with respect to the magnetic field.

$$\begin{pmatrix} \cos \Psi & -\sin \Psi & 0 \\ \sin \Psi & \cos \Psi & 0 \\ 0 & 0 & 1 \end{pmatrix} \begin{pmatrix} \kappa_{\parallel} & 0 & 0 \\ 0 & \kappa_{\perp} & \kappa_A \\ 0 & -\kappa_A & \kappa_{\perp} \end{pmatrix} \begin{pmatrix} \cos \Psi & \sin \Psi & 0 \\ -\sin \Psi & \cos \Psi & 0 \\ 0 & 0 & 1 \end{pmatrix} = \begin{pmatrix} \kappa_{\parallel} \cos^2 \Psi + \kappa_{\perp} \sin^2 \Psi & (\kappa_{\parallel} - \kappa_{\perp}) \sin \Psi \cos \Psi & -\kappa_A \sin \Psi \\ (\kappa_{\parallel} - \kappa_{\perp}) \sin \Psi \cos \Psi & \kappa_{\parallel} \sin^2 \Psi + \kappa_{\perp} \cos^2 \Psi & \kappa_A \cos \Psi \\ \kappa_A \sin \Psi & -\kappa_A \cos \Psi & \kappa_{\perp} \end{pmatrix}. \quad (7.35)$$

The small-scale downstream gradient scale size of the distribution function f points normal to the shock surface $\nabla f = f(r_G^{-1}, 0, 0)$. This gradient “picks out” the first row of the matrix in Equation (7.35).

The most fundamental approach for solving the Parker equation (7.1) is to assume infinitely large upstream and downstream plasma regions. If one takes x as the parameter along the shock normal, the Parker equation becomes

$$V \frac{\partial f}{\partial x} + \frac{\partial}{\partial x} \left[V \frac{v}{3} \frac{\partial f}{\partial v} + (\tilde{\kappa} \cdot \nabla f)_x \right] = 0. \quad (7.36)$$

Integrating this equation over x yields

$$V_1 f(0, v) = (V_2 - V_1) \frac{v}{3} \frac{\partial f}{\partial v}(0, v) \Rightarrow f(0, v) = f_0 v^{-\gamma}, \quad \gamma = \frac{3V_1}{V_1 - V_2}, \quad (7.37)$$

with 1 denoting the upstream region and 2 the downstream region. This is the standard distribution of first-order Fermi accelerated ions. It is based on the assumptions, that far away from the shock the distribution f has no gradient, that far upstream the distribution function vanishes, $f(-\infty, v) = 0$, and that the downstream distribution function is constant ($r_G \rightarrow \infty$), i.e. describing a particle distribution flushed away in diffusive equilibrium, and that the variation of the second term is dominated by the jump in speed from V_1 to V_2 at the shock.

However, it is necessary to add sources to the above equation in order to have any particles. These could be far upstream, $f(-\infty, v)$, and convected to the shock, or be near the shock, $f_S(v)$:

$$f(0, v) = \gamma v^{-\gamma} \int_{v_{\text{inj}}}^v (v')^{\gamma} [f(-\infty, v') + f_S(v')] \frac{dv'}{v'}. \quad (7.38)$$

Upstream from the shock ($x < 0$) the spatial distribution is given by

$$f(x, v) = f(-\infty, v) + [f(0, v) - f(-\infty, v)] \exp \left(\int_0^x \frac{V_1 dx'}{\kappa_1(x', v, A/Q)} \right). \quad (7.39)$$

Here, it is assumed that a single parameter κ_1 describes diffusion along the shock normal upstream from the shock. The diffusion parameter depends in general on speed, through the level of turbulence at the location x , and on speed v .

In Equation (7.38), the injection speed v_{inj} is introduced. For $v > v_{\text{inj}}$, the downstream diffusion speed is equal to the upstream convection speed V_1 , i.e. all particles convected into the shock are scattered back:

$$(\tilde{\kappa} \cdot \nabla f)_x = V_1 f \quad \rightarrow \quad \frac{\kappa_{\parallel}}{r_G} (\cos^2 \theta + \kappa_{\perp} \sin^2 \theta / \kappa_{\parallel}) = V_1 . \quad (7.40)$$

In this way, the downstream gradient scale r_G adjusts to balance a stationary situation at the shock. At high speeds the spatial diffusion parameter becomes large ($\kappa \rightarrow \infty$) and thus the gradient scale is large $r_G \rightarrow \infty$. The lower the speed, the smaller is κ , but r_G cannot be smaller than the gyroradius r_g or some other characteristic value. For $v = v_{\text{inj}}$ the gradient scale r_G reaches its smallest value; for $v < v_{\text{inj}}$ the diffusive acceleration no longer operates with full efficiency.

The diffusive streaming anisotropy is (Giacalone and Jokipii, 1999):

$$\delta := \frac{|3\tilde{\kappa} \cdot \nabla f|}{vf} = \frac{3V_1}{v} \left[1 + \frac{(\kappa_A / \kappa_{\parallel})^2 \sin^2 \Psi + (1 - \kappa_{\perp} / \kappa_{\parallel})^2 \sin^2 \Psi \cos^2 \Psi}{[(\kappa_{\perp} / \kappa_{\parallel}) \sin^2 \Psi + \cos^2 \Psi]^2} \right]^{1/2} . \quad (7.41)$$

If this anisotropy is small, then the Parker equation (7.1) can be applied and diffusive first-order Fermi acceleration operates as derived. It can be argued here whether the upstream or the downstream diffusion parameters must be entered to ensure that δ be small. As the downstream parameters of $\tilde{\kappa}_2$ are larger than those of $\tilde{\kappa}_1$, we tend to use $\tilde{\kappa}_2$ as a more stringent constraint.

7.B MHD-description of solar wind turbulence

The following derivation of the magnetohydrodynamic (MHD) model of plasma turbulence follows closely the work by Zhou and Matthaeus (1990). The properties of the plasma are described by the proton mass density $\rho(\mathbf{X}, t)$, the plasma velocity $\mathbf{V}(\mathbf{X}, t)$, and the magnetic field $\mathbf{B}(\mathbf{X}, t)$. We distinguish large scales \mathbf{X} and fluctuation scales \mathbf{x} and assume incompressibility. We have the mass continuity equation, the induction equation with diffusive term \mathbf{D}' , vanishing divergence of the magnetic field \mathbf{B} , and an equation of motion:

$$\begin{aligned} \dot{\rho} &= -\nabla \cdot (\rho \mathbf{V}), \quad \dot{\mathbf{B}} = \nabla \times (\mathbf{V} \times \mathbf{B}) + \mathbf{D}', \quad \nabla \cdot \mathbf{V} = 0, \quad \nabla \cdot \mathbf{B} = 0, \\ \rho \left[\dot{\mathbf{V}} + (\mathbf{V} \cdot \nabla) \mathbf{V} \right] &= -\nabla p + \mathbf{J} \times \mathbf{B} + \mathbf{D}, \end{aligned} \quad (7.42)$$

where p is the mechanical plasma pressure, and $\mathbf{J} = \mu_0 \nabla \times \mathbf{B}$ is the electric current density. Alternative forms of the equation of motion and the equation of induction without the dissipation terms are

$$\begin{aligned} \mathcal{D} \mathbf{V} - (\mu_0 \rho)^{-1} (\mathbf{B} \cdot \nabla) \mathbf{B} &= -\rho^{-1} \nabla p^{\text{T}}, \quad p^{\text{T}} = p + \mu_0^{-1} B^2, \\ \mathcal{D} \mathbf{B} - (\mathbf{B} \cdot \nabla) \mathbf{V} &= -(\nabla \cdot \mathbf{V}) \mathbf{B}, \quad \mathcal{D} := \partial_t + \mathbf{V} \cdot \nabla. \end{aligned} \quad (7.43)$$

We decompose the plasma properties into a mean part, typically varying on a spatial scale that corresponds to the heliocentric radial coordinate R , and a turbulent inertial part, typically ranging in spatial scale over more than three decades from a correlation scale $L_c \ll R$ down to the thermal ion gyroscale:

$$\mathbf{V} = \mathbf{U} + \mathbf{v}, \quad \mathbf{B} = \mathbf{B}_0 + \mathbf{b}, \quad \rho = \rho_0 + \delta\rho, \quad p^{\text{T}} = p_0^{\text{T}} + \delta p^{\text{T}}, \quad \mathcal{D} := \partial_t + \mathbf{U} \cdot \nabla. \quad (7.44)$$

It is assumed that the fluctuating part of the turbulence part is incompressible, i.e. $\delta\rho = 0$, an assumption which is not necessarily true but is made in many models on solar wind MHD-turbulence. The average $\langle \dots \rangle$ of a turbulent component vanishes, while the average of the product of two turbulent components does not vanish in general. Averaging of the equations of motion and induction yields

$$\begin{aligned} \mathcal{D}\mathbf{U} + \langle (\mathbf{v} \cdot \nabla) \mathbf{v} \rangle - (\mu_0 \rho)^{-1} [(\mathbf{B}_0 \cdot \nabla) \mathbf{B}_0 + \langle (\mathbf{b} \cdot \nabla) \mathbf{b} \rangle] &= -\rho_0^{-1} \nabla p_0^T, \\ \mathcal{D}\mathbf{B}_0 + \langle (\mathbf{v} \cdot \nabla) \mathbf{b} \rangle - [(\mathbf{B}_0 \cdot \nabla) \mathbf{U} + \langle (\mathbf{b} \cdot \nabla) \mathbf{v} \rangle] \\ - [(\nabla \cdot \mathbf{U}) \mathbf{B}_0 + \langle (\nabla \cdot \mathbf{v}) \mathbf{b} \rangle] &= 0. \end{aligned} \quad (7.45)$$

The difference between Equations (7.43) and (7.45) yields

$$\begin{aligned} \mathcal{D}\mathbf{v} + (\mathbf{v} \cdot \nabla) \mathbf{U} - (\mu_0 \rho)^{-1} [(\mathbf{B}_0 \cdot \nabla) \mathbf{b} + (\mathbf{b} \cdot \nabla) \mathbf{B}_0] &= -\rho^{-1} \nabla \delta p^T + \mathbf{N}^v; \\ \mathcal{D}\mathbf{b} + (\mathbf{v} \cdot \nabla) \mathbf{B}_0 - (\mathbf{B}_0 \cdot \nabla) \mathbf{v} - (\mathbf{b} \cdot \nabla) \mathbf{U} &= -(\nabla \cdot \mathbf{U}) \mathbf{b} - (\nabla \cdot \mathbf{v}) \mathbf{B}_0 + \mathbf{N}^b; \\ \mathbf{N}^v &= -[(\mathbf{v} \cdot \nabla) \mathbf{v} - \langle (\mathbf{v} \cdot \nabla) \mathbf{v} \rangle] + (\mu_0 \rho)^{-1} [(\mathbf{b} \cdot \nabla) \mathbf{b} - \langle (\mathbf{b} \cdot \nabla) \mathbf{b} \rangle]; \\ \mathbf{N}^b &= -[(\mathbf{v} \cdot \nabla) \mathbf{b} - \langle (\mathbf{v} \cdot \nabla) \mathbf{b} \rangle] + [(\mathbf{b} \cdot \nabla) \mathbf{v} - \langle (\mathbf{b} \cdot \nabla) \mathbf{v} \rangle]. \end{aligned} \quad (7.46)$$

We have neglected non-averaged products of “small” variables \mathbf{v} and \mathbf{b} . In a similar fashion one obtains

$$\nabla \cdot \rho \mathbf{v} = 0. \quad (7.47)$$

7.B.1 Description of MHD turbulence by Elsässer variables

Using the Elsässer variables

$$\mathbf{z}^\pm = \mathbf{v} \pm \frac{1}{\sqrt{\mu_0 \rho}} \mathbf{b} \quad (7.48)$$

Equations (7.46) become

$$\begin{aligned} \frac{\partial \mathbf{z}^\pm}{\partial t} + (\mathbf{U} \mp \mathbf{V}_A) \cdot \nabla \mathbf{z}^\pm + \frac{1}{2} (\mathbf{z}^\pm - \mathbf{z}^\mp) \nabla \cdot \left(\frac{\mathbf{U}}{2} \pm \mathbf{V}_A \right) \\ + \mathbf{z}^\mp \cdot \left(\nabla \mathbf{U} \pm \frac{1}{\sqrt{\mu_0 \rho}} \nabla \mathbf{B}_0 \right) &= -\frac{1}{\rho} \nabla p + \mathbf{N}_0^\pm; \\ \mathbf{N}_0^\pm &= \mathbf{N}^v \pm \frac{1}{\sqrt{\mu_0 \rho}} \mathbf{N}^b. \end{aligned} \quad (7.49)$$

In N_b the term $(\nabla \cdot \mathbf{v}) \mathbf{b} - \langle (\nabla \cdot \mathbf{v}) \mathbf{b} \rangle$ has been set to zero because the turbulence is assumed to be incompressible, i.e. $(\nabla \cdot \mathbf{v}) = 0$.

The above equation is derived in the following way:

$$\begin{aligned} \frac{\partial \mathbf{v}}{\partial t} \pm \frac{1}{\sqrt{\mu_0 \rho}} \frac{\partial \mathbf{b}}{\partial t} &= \frac{\partial \mathbf{z}^\pm}{\partial t}; \\ (\mathbf{U} \cdot \nabla) \mathbf{v} \pm \frac{1}{\sqrt{\mu_0 \rho}} (\mathbf{U} \cdot \nabla) \mathbf{b} &= (\mathbf{U} \cdot \nabla) \mathbf{z}^\pm \mp \mathbf{b} (\mathbf{U} \cdot \nabla) \frac{1}{\sqrt{\mu_0 \rho}}; \\ (\mathbf{v} \cdot \nabla) \mathbf{U} \pm \frac{1}{\sqrt{\mu_0 \rho}} (-\mathbf{b} \cdot \nabla) \mathbf{U} &= (\mathbf{z}^\mp \cdot \nabla) \mathbf{U}; \end{aligned}$$

$$\begin{aligned}
-\frac{(\mathbf{B}_0 \cdot \nabla) \mathbf{b}}{\mu_0 \rho} \pm \frac{1}{\sqrt{\mu_0 \rho}} (-\mathbf{B}_0 \cdot \nabla) \mathbf{v} &= \mp (\mathbf{V}_A \cdot \nabla) \mathbf{z}^\pm + \mathbf{b} (\mathbf{V}_A \cdot \nabla) \frac{1}{\sqrt{\mu_0 \rho}} ; \\
(\mathbf{b} \cdot \nabla) \mathbf{B}_0 \pm \frac{1}{\sqrt{\mu_0 \rho}} (\mathbf{v} \cdot \nabla) \mathbf{B}_0 &= \pm \frac{1}{\sqrt{\mu_0 \rho}} (\mathbf{z}^\mp \cdot \nabla) \mathbf{B}_0 .
\end{aligned} \tag{7.50}$$

The first line is valid because $\dot{\rho} = 0$ ($\delta\rho = 0$ or $\rho = \langle\rho\rangle$). The last term of the fourth line yields

$$\mathbf{b} (\mathbf{V}_A \cdot \nabla) \frac{1}{\sqrt{\mu_0 \rho}} = \frac{\mathbf{b}}{\sqrt{\mu_0 \rho}} (\mathbf{B}_0 \cdot \nabla) \frac{1}{\sqrt{\mu_0 \rho}} = \frac{1}{2} (\mathbf{z}^\pm - \mathbf{z}^\mp) (\pm \nabla \cdot \mathbf{V}_A) \tag{7.51}$$

because $\nabla \cdot \mathbf{B}_0 = 0$.

The last term of the fourth line and the term $\pm (\nabla \cdot \mathbf{U}) \mathbf{b} / \sqrt{\mu_0 \rho}$ remaining from the second equation in (7.46) are added:

$$\begin{aligned}
\mp \mathbf{b} (\mathbf{U} \cdot \nabla) \frac{1}{\sqrt{\mu_0 \rho}} \pm \frac{\mathbf{b} (\nabla \cdot \mathbf{U})}{\sqrt{\mu_0 \rho}} &= \frac{1}{2} (\mathbf{z}^\pm - \mathbf{z}^\mp) \left(\nabla \cdot \frac{\mathbf{U}}{2} \right) \\
\text{because of } \frac{\mathbf{U}}{\rho} \cdot \nabla \rho = -\nabla \cdot \mathbf{U} \text{ i.e. } \nabla \cdot (\rho \mathbf{U}) &= 0 .
\end{aligned} \tag{7.52}$$

7.B.2 Assumptions for the solar wind turbulence

We now mainly follow the work by Zank et al. (1996a). With $V_A \ll U$, the equations reduce to

$$\begin{aligned}
\frac{\partial \mathbf{z}^\pm}{\partial t} + \mathbf{U} \cdot \nabla \mathbf{z}^\pm + \frac{1}{2} \mathbf{z}^\pm \nabla \cdot \frac{\mathbf{U}}{2} + \mathbf{z}^\mp \cdot \mathcal{M} &= N \mathbf{L}^\pm + \mathbf{S}^\pm \\
\mathcal{M} &= \left[\nabla \otimes \mathbf{U} - \frac{1}{2} \mathbf{I} \nabla \cdot \frac{\mathbf{U}}{2} \right] .
\end{aligned} \tag{7.53}$$

The dissipation and source terms on the r.h.s of the first line are somewhat rewritten and will be evaluated later.

In order to obtain an equation for the evolution of turbulent power, one needs to multiply the above equation by \mathbf{z}^\pm and to average over small scale fluctuations. The tensor \mathcal{M} is then a contraction tensor for the Elsässer variables $\mathbf{z}^\pm \mathcal{M} \mathbf{z}^\mp$. However, the heliosphere will usually be described in heliocentric coordinates, while the Elsässer variables refer to a coordinate system that is fixed to the heliospheric magnetic field, which in the most simple approach is described by a Parker spiral with Parker angle Ψ of the magnetic field with respect to the radial direction of the heliosphere. Therefore the contraction \mathcal{M} needs to include the coordinate transformation from heliocentric coordinates to the coordinate system aligned to the large-scale heliospheric magnetic field. This is done by a rotation

$$\mathcal{O} = \begin{pmatrix} \cos \Psi & 0 & \sin \Psi \\ 0 & 1 & 0 \\ -\sin \Psi & 0 & \cos \Psi \end{pmatrix} \tag{7.54}$$

We can reduce the mathematical effort by constraining ourselves to certain symmetries of turbulence. Three types of turbulence are most often discussed in the

literature: (1) isotropic turbulence, (2) turbulence in slab geometry with the fluctuation amplitudes \mathbf{v} and \mathbf{b} perpendicular to the ambient magnetic field \mathbf{B}_0 and the wave vector \mathbf{k} parallel to \mathbf{B}_0 , and (3) the so-called 2D-MHD turbulence (Bieber et al. (1996) with $\mathbf{k} \perp \mathbf{B}_0$ and \mathbf{v} and \mathbf{b} mutually perpendicular to both \mathbf{k} and \mathbf{B}_0 but isotropic distribution of the wave vectors in the plane orthogonal to \mathbf{B}_0 . This enables us to introduce projection matrices \mathcal{P}_S and \mathcal{P}_{2D} for symmetric and slab/2D turbulence, respectively, in the frame aligned with \mathbf{B}_0 :

$$\mathcal{P}_S = \frac{1}{3} \begin{pmatrix} 1 & 0 & 0 \\ 0 & 1 & 0 \\ 0 & 0 & 1 \end{pmatrix}; \quad \mathcal{P}_{2D} = \frac{1}{2} \begin{pmatrix} 0 & 0 & 0 \\ 0 & 1 & 0 \\ 0 & 0 & 1 \end{pmatrix}. \quad (7.55)$$

The action of the contraction tensor \mathcal{M}_B and the projection tensor $\mathcal{P}_{2D;B}$ needs to be transformed from the coordinate system aligned to \mathbf{B}_0 to the heliocentric coordinate system, where the contraction tensor is denoted by \mathcal{M}_H and the projection tensor $\mathcal{P}_{2D;H}$:

$$\begin{aligned} \mathbf{z}_B^{\pm;T} \mathcal{P}_{2D;B}^T \mathcal{M}_B \mathbf{z}_B^{\mp} &= \mathbf{z}_B^{\pm;T} \mathcal{O}^T \mathcal{O} \mathcal{P}_{2D;B}^T \mathcal{O}^T \mathcal{O} \mathcal{M}_B \mathcal{O}^T \mathcal{O} \mathbf{z}_B^{\mp} = \mathbf{z}_H^{\pm;T} \mathcal{P}_{2D;H}^T \mathcal{M}_H \mathbf{z}_H^{\mp;T} \\ \mathbf{z}_H^{\pm;T} &= \mathbf{z}_B^{\pm;T} \mathcal{O}^T; \quad \mathcal{P}_{2D;H}^T = \mathcal{O} \mathcal{P}_{2D;B}^T \mathcal{O}^T; \quad \mathcal{M}_H = \mathcal{O} \mathcal{M}_B \mathcal{O}^T; \\ \mathcal{P}_{2D;H}^T &= \begin{pmatrix} \sin^2 \Psi & 0 & \sin \Psi \cos \Psi \\ 0 & 1 & 0 \\ \sin \Psi \cos \Psi & 0 & \cos^2 \Psi \end{pmatrix}. \end{aligned} \quad (7.56)$$

The superscript T denotes a transposed tensor. The subscripts H and B at the Elsässer variables denote the heliocentric coordinate system and that aligned with the ambient magnetic field \mathbf{B}_0 , respectively. We derive the tensor \mathcal{M}_H (Equation 7.53) in heliocentric coordinates:

$$\begin{aligned} \nabla \cdot \mathbf{U} &= \frac{1}{r^2} \frac{\partial}{\partial r} (r^2 U) + \frac{1}{r} \frac{\partial U}{\partial \theta} + \frac{1}{r \sin \theta} \frac{\partial U}{\partial \Psi} \quad \text{and} \\ \nabla \otimes \mathbf{U} &= \begin{pmatrix} \partial_r U & 0 & 0 \\ r^{-1} \partial_\theta U & 0 & 0 \\ (r \sin \theta)^{-1} \partial_\Psi U & 0 & 0 \end{pmatrix} \quad \text{if } \mathbf{U} = U \mathbf{e}_r \quad \Rightarrow \\ \mathcal{M} &= \begin{pmatrix} 1 & 0 & 0 \\ 0 & -1 & 0 \\ 0 & 0 & -1 \end{pmatrix} \frac{U}{2r} + \begin{pmatrix} -1 & 0 & 0 \\ 0 & 1 & 0 \\ 0 & 0 & 1 \end{pmatrix} \frac{1}{2} \frac{\partial U}{\partial r} \\ &+ \begin{pmatrix} 0 & 0 & 0 \\ 1 & 0 & 0 \\ 0 & 0 & 0 \end{pmatrix} \frac{1}{r} \frac{\partial U}{\partial \theta} + \begin{pmatrix} 0 & 0 & 0 \\ 0 & 0 & 0 \\ 1 & 0 & 0 \end{pmatrix} \frac{1}{r \sin \theta} \frac{\partial U}{\partial \Psi}. \end{aligned} \quad (7.57)$$

After multiplying the contraction term by \mathbf{z}^\pm and averaging over the short fluctuation scales, we obtain

$$\left(\frac{1}{3} \frac{U}{2r} - \frac{1}{3} \frac{1}{2} \frac{\partial U}{\partial r} \right) \langle \mathbf{z}^- \cdot \mathbf{z}^+ \rangle =: M_S \langle \mathbf{z}^- \cdot \mathbf{z}^+ \rangle \quad (7.58)$$

in the case of isotropic turbulence and

$$\left[\frac{\cos^2 \Psi}{2} \left(\frac{U}{r} - \frac{\partial U}{\partial r} \right) + \frac{1}{2} \frac{\partial U}{\partial \theta} + \frac{1}{2 \sin \theta} \frac{\partial U}{\partial \Psi} \right] \langle \mathbf{z}^- \cdot \mathbf{z}^+ \rangle =: M_{2D} \langle \mathbf{z}^- \cdot \mathbf{z}^+ \rangle \quad (7.59)$$

for the 2D and the slab case, if $\langle z_i^\pm z_j^\mp \rangle = 0$ for $i \neq j$ Zank et al. (1996a).

By multiplying Equations (7.53) for the evolution of \mathbf{z}^+ and \mathbf{z}^- by \mathbf{z}^+ and \mathbf{z}^- , respectively, we obtain two equations

$$\frac{1}{2}\mathcal{D}'\langle(\mathbf{z}^\pm)^2\rangle + M_{S/2D}\langle\mathbf{z}^- \cdot \mathbf{z}^+\rangle = S^\pm + D^\pm, \quad \mathcal{D}' = \left(\frac{\partial}{\partial t} + \nabla \cdot \frac{\mathbf{U}}{2} + \mathbf{U} \cdot \nabla\right), \quad (7.60)$$

where S and D denote source and dissipation terms and \mathcal{D}' is a differential operator. Multiplying Equation (7.53) for \mathbf{z}^+ by \mathbf{z}^- and that for \mathbf{z}^- by \mathbf{z}^+ and adding the resulting equations yields

$$\mathcal{D}'\langle\mathbf{z}^- \cdot \mathbf{z}^+\rangle + M_{S/2D}\left[\langle(\mathbf{z}^+)^2\rangle + \langle(\mathbf{z}^-)^2\rangle\right] = S_m + D_m. \quad (7.61)$$

The Elsässer variables \mathbf{z}^\pm are related to kinetic and magnetic energy E_v and E_b and to the cross helicity H^C through

$$\begin{aligned} E = E_v + E_b &= \frac{1}{4}\left[\langle(\mathbf{z}^+)^2\rangle + \langle(\mathbf{z}^-)^2\rangle\right]; \quad E^R = E_v - E_b = \frac{1}{2}\langle\mathbf{z}^- \cdot \mathbf{z}^+\rangle; \\ H^C = E^+ - E_- &= \frac{1}{4}\left[\langle(\mathbf{z}^+)^2\rangle - \langle(\mathbf{z}^-)^2\rangle\right]. \end{aligned} \quad (7.62)$$

Therefore, Equations (7.60) and (7.61) represent

$$\begin{aligned} \mathcal{D}'(E_v + E_b) + 2M_{S/2D}(E_v - E_b) &= \frac{1}{2}(S^+ + S^- + D^+ + D^-), \\ \mathcal{D}'(E_v - E_b) + 2M_{S/2D}(E_v + E_b) &= \frac{1}{2}(S_1 + D_1), \end{aligned} \quad (7.63)$$

where the difference of these two equations describes the evolution of E_b and the sum the evolution of E_v . In the case of constant Alfvén ratio $r_A = E_v/E_b$, the first equation can be written as

$$\mathcal{D}'E_b + 2M\sigma_D E_b = S' + D' \quad \text{with} \quad \sigma_D = (r_A - 1)/(r_A + 1). \quad (7.64)$$

We introduce the parameter $\Gamma_{\text{iso}} = 2M_{\text{iso}}\sigma_D$ for the contraction term of isotropic turbulence (7.58) and $\Gamma_{2D} = 2M_{S/2D}\sigma_D$ for slab/2D turbulence (7.59):

$$\Gamma_{\text{iso}} = -\frac{1}{3}\sigma_D > 0 \quad \text{and} \quad \Gamma_{2D} = -\sigma_D \cos^2 \Psi > 0, \quad (7.65)$$

where Ψ is the angle between the magnetic field and the plasma flow.

With the parameter Γ , Equation (7.64) takes the form

$$\mathcal{D}''E_b = S' + D'; \quad \mathcal{D}'' = \left(\frac{\partial}{\partial t} + \nabla \cdot \frac{\mathbf{U}}{2} + \mathbf{U} \cdot \nabla\right) - \Gamma \frac{U}{r} \quad (7.66)$$

for a stationary flow.

7.B.3 Dissipation

Now we need to incorporate the source and dissipation terms. Rather than going through a detailed treatment of the dissipation terms, we use the dimension and scale invariance arguments of von Karman and Howarth (1938, see also Matthaeus et al., 1996):

$$\frac{\partial v^2}{\partial t} = -\alpha \frac{v^3}{l_c} + S, \quad \frac{\partial l_c}{\partial t} = \beta v, \quad v^2 l_c^{\alpha/\beta} = \text{const.}, \quad (7.67)$$

where S is the source term. The dissipation is assumed to depend on a typical length scale l_c (correlation length) of the turbulence and on the third power of the speed. If α and β are dimensionless parameters, the above equations have terms of equal dimensions. As is easily verified, the solutions of the above equations are

$$\begin{aligned} v(t) &= v_0 [1 + A(t - t_0)]^{-\alpha/(\alpha+2\beta)}, \\ l_c(t) &= l_{c;0} [1 + A(t - t_0)]^{2\beta/(\alpha+2\beta)}, \quad A^{-1} = \frac{2}{\alpha + 2\beta} \frac{l_{c;0}}{v_0}. \end{aligned} \quad (7.68)$$

For $t \gg A^{-1}$, these solutions are power laws. The typical behaviour of a fluctuating variable is that $v^2(t) \rightarrow t$, and thus $\alpha = 2\beta$. As the scales for l_c and v can be changed independently, we should have $A^{-1} = l_{c;0}/v_0$, and thus $\alpha + 2\beta = 2$. This yields $\alpha = 1$ and $\beta = 1/2$.

We transfer the above principle to the case of expanding hydromagnetic systems by postulating that

$$\begin{aligned} \mathcal{D}'(E_b l_c^2) = 0 &\Rightarrow l_c^2 \mathcal{D}' E_b + 2l_c E_b (\partial_t + \mathbf{U} \cdot \nabla) l_c = 0 \Rightarrow \\ &-\frac{E_b^{3/2}}{l_c} + S + 2l_c E_b \left(\frac{\partial}{\partial t} + \mathbf{U} \cdot \nabla + \Gamma \frac{U}{r} \right) l_c = 0 \Rightarrow \\ &\left(\frac{\partial}{\partial t} + \mathbf{U} \cdot \nabla + \Gamma \frac{U}{r} \right) l_c = \frac{E_b^{1/2}}{2l_c} - \frac{S l_c}{2E_b}. \end{aligned} \quad (7.69)$$

The second line follows because the term $\nabla \cdot \mathbf{U}/2$ is only applied once as a scalar, while for the other differential operator the product rule has to be used. The third line follows from Equation (7.66).

For a stationary situation, we have the set of equations:

$$\begin{aligned} \left(\frac{\partial}{\partial t} + \nabla \cdot \frac{\mathbf{U}}{2} + \mathbf{U} \cdot \nabla - \Gamma \frac{U}{r} \right) E_b &= -\frac{E_b^{3/2}}{l_c} + S; \\ \left(\mathbf{U} \cdot \nabla + \Gamma \frac{U}{r} \right) l_c &= \frac{E_b^{1/2}}{2} - \frac{l_c S}{2E_b}. \end{aligned} \quad (7.70)$$

Bibliography

Acuña et al.: 2006, Proc. 5th IGPP Conf. *The Physics of the Inner Heliosheath: Voyager Observations, Theory, and Future Prospects*, Waikiki Beach, Hawaii, 3–9 March 2006, in press.

- Alexashov, D.B., Chalov, S.V., Myasnikov, A.V., Izmodenov, V.V., and Kallenbach, R.: 2004, 'The dynamical role of anomalous cosmic rays in the outer heliosphere', *Astron. Astrophys.* **420**, 729–736.
- Bamert, K., Kallenbach, R., Ness, N.F., Smith, C.W., Terasawa, T., Hilchenbach, M., Wimmer-Schweingruber, R.F., and Klecker, B.: 2004, 'Hydromagnetic wave excitation upstream of an interplanetary traveling shock', *Astrophys. J.* **601**, L99–L102.
- Baumjohann, W., and Treumann, R.A.: 1996, *Basic Space Plasma Physics*, Imperial College Press, London.
- Bieber, J.W., Wanner, W., and Matthaeus, W.H.: 1996, 'Dominant two-dimensional solar wind turbulence with implications for cosmic ray transport', *J. Geophys. Res.* **101**, 2'511–2'522.
- Burlaga, L.F., Ness, N.F., Acuña, M.H., Lepping, R.P., Connerney, J.E.P., Stone, E.C., and McDonald, F.B.: 2005, 'Crossing the termination shock into the heliosheath: magnetic fields', *Science* **309**, 2027–2029.
- Bykov, A.M., and Toptygin, I.N.: 1993, *Phys.-Uspekhi* **36**, 1020.
- Chalov, S.V.: 1993, 'Longitudinal distribution of anomalous hydrogen near the solar wind termination shock', *Planet. Space Sci.* **41**, 133.
- Chalov, S.V.: 2000, 'Acceleration of pick-up ions at the solar wind termination shock', *Astrophys. Space Sci.* **274**, 25.
- Chalov, S.V.: 2005, 'Acceleration of interplanetary pick-up ions and anomalous cosmic rays', *Adv. Space Res.* **35**, 2106.
- Chalov, S.V., and Fahr, H.J.: 1996, 'Reflection of pre-accelerated pick-up ions at the solar wind termination shock: the seed for Anomalous Cosmic Rays', *Solar Phys.* **168**, 389.
- Chalov, S.V., and Fahr, H.J.: 2000, 'Pick-up ion acceleration at the termination shock and the post-shock pick-up ion energy distribution', *Astron. Astrophys.* **360**, 381.
- Chalov, S.V., Fahr, H.J., and Izmodenov, V.: 1997, *Astron. Astrophys.* **320**, 659.
- Chalov, S.V., Alexashov, D.B., and Fahr, H.J.: 2006, 'Interstellar pickup protons and solar wind heating in the outer heliosphere', *Astron. Lett.* **32**, 206–213.
- Decker, R.B., Krimigis, S.M., Roelof, E.C., Hill, M.E., Armstrong, T.P., Gloeckler, G., Hamilton, D.C., and Lanzerotti, L.J.: 2005, 'Voyager 1 in the foreshock, termination shock, and heliosheath', *Science* **309**, 2020–2024.
- Fisk, L.A.: turbulent cascade.
- Galli, *et al.*: 2006, 'Direct measurements of energetic neutral hydrogen in the interplanetary medium', *Astrophys. J.* **644**, 1317–1325.
- Giacalone, J. and Jokipii, J.R.: 1999, 'The transport of cosmic rays across a turbulent magnetic field', *Astrophys. J.* **520**, 204–214.
- Gloeckler, G.: 2003, 'Ubiquitous suprathermal tails on the solar wind and pickup ion distributions', *Solar Wind 10*, AIP Conf. Proc. **679**, pp. 583–588.
- Gruntman, M., Roelof, E.C., Mitchell, D.G., Fahr, H.J., Funsten, H.O., and McComas, D.J.: 2001, 'Energetic neutral atom imaging of the heliospheric boundary region', *J. Geophys. Res.* **106**, 15'767–15'782.
- Horbury, T.S. and Balogh, A.: 2001, 'Evolution of magnetic field fluctuations in high-speed solar wind streams: Ulysses and Helios observations', *J. Geophys. Res.* **106**, 15'929–15'940.

- Isenberg, P.A., Smith, C.W., and Matthaeus, W.H.: 2003, ‘Turbulent heating of the distant solar wind by interstellar pickup protons’, *Astrophys. J.* **592**, 564–573.
- Jokipii, J.R.: 1966, ‘Cosmic-ray propagation. I. Charged particles in a random magnetic field’, *Astrophys. J.* **146**, 480–487.
- Jokipii, J.R., and Kota, J.: 1989, ‘The polar heliospheric magnetic field’, *Geophys. Res. Lett.* **16**, 1–4.
- Kallenbach, R., Hilchenbach, M., Chalov, S.V., Le Roux, J.A., and Bamert, K.: 2005, ‘On the injection problem at the solar wind termination shock’, *Astron. Astrophys.* **439**, 1–22.
- Lee, M.A., Shapiro, V.D., and Sagdeev, R.Z.: 1996, ‘Pickup ion energization by shock surfing’, *J. Geophys. Res.* **101**, 4777.
- le Roux, J.A., Fichtner, H., and Zank, G.P., ‘Self-consistent acceleration of multiply reflected pickup ions at a quasi-perpendicular solar wind termination shock: a fluid approach’, *J. Geophys. Res.* **105**, 12557–12578.
- Matsukiyo, S., and Scholer, M.: 2003, ‘Modified two-stream instability in the foot of high Mach number quasi-perpendicular shocks’, *J. Geophys. Res.* **108**, SMP 19-1, CiteID 1459, DOI 10.1029/2003JA010080.
- Matthaeus, W.H., Zank, G.P., and Oughton, S.: 1996, ‘Phenomenology of hydro-magnetic turbulence in a uniformly expanding medium’, *J. Plasma Physics* **56**, 659–675.
- McComas, D.J., and Schwadron, N.A.: 2006, ‘An explanation of the Voyager paradox: Particle acceleration at a blunt termination shock’, *Geophys. Res. Lett.* **33**, CiteID L04102.
- Möbius, E., and Kallenbach, R.: 2005, ‘Acceleration in the heliosphere’, in J. Geiss and B. Hultqvist (eds.), *The solar system and beyond: ten years of ISSI*. ISSI scientific report, SR-003 Bern, Switzerland: The International Space Science Institute, p. 165.
- Ness, N.F.: 2006, ‘Heliospheric magnetic fields and termination shock crossing: Voyager 1’, this volume.
- Sagdeev, R.Z.: 1966, ‘Cooperative phenomena and shock waves in collisionless plasmas’, in M.A. Leontovich (ed.), *Reviews of Plasma Physics*, vol. 4, Consultants Bur., New York, p. 23.
- Scholer, M., Shinohara, I., and Matsukiyo, S.: 2003, ‘Quasi-perpendicular shocks: Length scale of the cross-shock potential, shock reformation, and implication for shock surfing’, *J. Geophys. Res.* **108**, 1014, doi:10.1029/2002JA009515.
- Stone, E.C., Cummings, A.C., McDonald, F.B., Heikkila, B.C., Lal, N., and Weber, W.R.: 2005, ‘Voyager 1 explores the termination shock region and the heliosheath beyond’, *Science* **309**, 2017–2020.
- Tidman, D.A., and Krall, N.A.: 1971, ‘Shock waves in collisionless Plasmas’, in S.C. Brown (ed.), *Series in Plasma Physics*, Wiley, New York, pp. 29–38.
- Tu, C.-Y., Marsch, E., and Rosenbauer, H.: 1990, ‘The dependence of MHD turbulence spectra on the inner solar wind stream structure near solar minimum’, *Geophys. Res. Lett.* **17**, 283–286.
- Vainio, R. and Schlickeiser, R.: 1999, ‘Self-consistent Alfvén-wave transmission and test-particle acceleration at parallel shocks’, *Astron. Astrophys.* **343**, 303–311.

- Vasyliunas, V.M., and Siscoe, G.L.: 'On the flux and the energy spectrum of interstellar ions in the solar system' *J. Geophys. Res.* **81**, 1247–1252.
- von Karman, T., and Howarth, L.: 1938, 'On the statistical theory of isotropic turbulence', *Proc. R. Soc. London* **164**, 192.
- Warren, J.S., Hughes, J.P., Badenes, C., Ghavamian, P., McKee, C.F., Moffett, D., Plucinsky, P.P., Rakowski, C., Reynoso, E., and Slane, P.: 2005, 'Cosmic-ray acceleration at the forward shock in Tycho's supernova remnant: evidence from Chandra X-ray observations', *Astrophys. J.* **634**, 376–389.
- Wu, C.S., and Davidson, R.C.: 1972, 'Electromagnetic instabilities produced by neutral-particle ionization in interplanetary space', *J. Geophys. Res.* **77**, 5399–5406.
- Zank, G.P., Matthaeus, W.H., and Smith, C.W.: 1996a, 'Evolution of turbulent magnetic fluctuation power with heliospheric distance', *J. Geophys. Res.* **101**, 17'093–17'107.
- Zank, G.P., Pauls, H.L., Cairns, I.H., and Webb, G.M.: 1996b, 'Interstellar pickup ions and quasi-perpendicular shocks: Implications for the termination shock', *J. Geophys. Res.* **101**, 457.
- Zhou, Y., and Matthaeus, W.H.: 1990, 'Transport and turbulence modeling of solar wind fluctuations', *J. Geophys. Res.* **95**, 10'291–10'311.